Accepted Manuscript

Geological Society, London, Special Publications

Integration of tectonic geomorphology and crustal structure across the active oblique collisional zone on the island of Hispaniola, northeastern Caribbean

Lei Sun, Paul Mann and Dale E. Bird

DOI: https://doi.org/10.1144/SP504-2019-242

Received 4 December 2019
Revised 16 April 2020
Accepted 28 April 2020

Sun, Lei, Mann, P., and Bird, D. E., 2020, Integration of tectonic geomorphology and crustal structure across the active oblique collisional zone on the island of Hispaniola, northeastern Caribbean: in, Davison, I., Hull, J. N. F., and Pindell, J. (editors), The basin, orogens and evolution of the southern Gulf of Mexico and northern Caribbean: Geological Society, London, Special Publications, v. 504.

Integration of tectonic geomorphology and crustal structure across the active oblique collisional zone on the island of Hispaniola, northeastern Caribbean

TECTONIC GEOMORPHOLOGY & CRUSTAL STRUCTURE OF HISPANIOLA

LEI SUN [1, *], PAUL MANN [1], & DALE E. BIRD [1, 2]

[1] Department of Earth and Atmospheric Sciences, University of Houston, 3607 Cullen Blvd, Houston, TX 77204, USA

[2] Bird Geophysical, 16903 Clan Macintosh, Houston, TX 77084, USA

ORCIDs: LS 0000-0002-9610-5266; PM 0000-0002-6221-3533

* Correspondence: lsun10@uh.edu

Abstract

Active tectonic deformation and seismicity of Hispaniola define a 250-km-wide, oblique collisional zone between the Bahamas, the island arc of Hispaniola, and the Caribbean Large Igneous Province (CLIP). To reflect how collision is accommodated within Hispaniola, we calculate river normalized steepness and terrain surface roughness to reveal areas of the most active uplift within central and western Hispaniola compared to eastern Hispaniola. We use gravity modelling to show thickness variations in the main crustal types in the convergent zone: 1) 33-45-km-thick arc crust in central and western Hispaniola; 2) 15-25-km-thick oceanic crust beneath the Bahamas north of Hispaniola; 3) 5-8-km thick Atlantic oceanic crust northeast of Hispaniola, and 4) 6-16-km-thick CLIP south of Hispaniola. Intermediate to deep earthquakes beneath eastern Hispaniola indicate active southwestward subduction of normal oceanic crust and northward subduction of the CLIP. We interpret that the west-to-east geomorphological and crustal variations within Hispaniola as the result of an along-strike transition from crustal shortening without subduction between the Bahamas and arc crust in central and western Hispaniola to subduction of the North American and Caribbean plates beneath eastern Hispaniola. Crustal shortening in central and western Hispaniola produces fault-bounded basins with sufficient clastic infill to produce hydrocarbon maturity.

Keywords

Tectonic geomorphology; gravity modelling; crustal structure; Hispaniola; oblique subduction; oblique collision

The island of Hispaniola is part of the Greater Antilles in the northeastern Caribbean and is divided into two countries: Haiti occupies the western third of the island and the Dominican Republic occupying the eastern two-thirds of the island. Hispaniola straddles the 250-km-wide North American-Caribbean active plate boundary and is obliquely convergent in a left-lateral sense (Mann *et al.* 2002; Calais *et al.* 2016) (Fig. 1).

The collisional zone in Hispaniola is formed by the oblique juxtaposition of four crustal elements on the North American and Caribbean plates: 1) the Mesozoic to recent, largely submarine, 2-5-km-thick Bahamas carbonate platform on the North American plate that is underlain by 15-20-km-thick oceanic crust and seamounts (Uchupi *et al.* 1971); 2) the normal-thickness Mesozoic oceanic crust to the east of the Bahamas (Dolan *et al.* 1998; Rodríguez-Zurrunero *et al.* 2019); 3) the Late Cretaceous Caribbean Large Igneous Province (CLIP) with crustal thicknesses of 8-20 km occupies the Caribbean plate south of Hispaniola (Mauffret *et al.* 1994; Diebold *et al.* 1999); and 4) the Cretaceous to Eocene island arc of the Caribbean with crustal thicknesses of 25-45 km occupies the central collisional and subduction plate boundary between the two obliquely-colliding plates (Corbeau *et al.* 2017; Núñez *et al.* 2019).

The island arc basement of Hispaniola can be subdivided into three active microplates that are known from GPS geodesy: North Hispaniola microplate along the northern margin of the island, Hispaniola microplate in the central and eastern part of the island, and Gonave microplate in the southern and southwestern part of the island (Benford *et al.* 2012) (Fig. 1). The Septentrional-Oriente fault zone (Prentice *et al.* 1993; Leroy *et al.* 2015) separates the Hispaniola and Gonave microplates from the North Hispaniola microplate (Fig. 1). Hispaniola microplate and Gonave microplate are bounded by large thrust faults in western Hispaniola (Mann *et al.* 1991b) (Fig. 1). Hispaniola microplate bounds Puerto Rico and Virgin Islands microplate (Masson & Scanlon 1991) at the Mona passage (Fig. 1). The Enriquillo-Plantain Garden fault zone (EPGFZ; Bowin 1975; Mann *et al.* 1984) and Muertos Trough separates Hispaniola microplate and Gonave microplate from CLIP in the south (Fig. 1). Tectonic deformations of Hispaniola are characterized by left-lateral strike-slip motion along the two major east-west and west-northwest-striking left-lateral strike-slip fault zones separated by an area of northwest-oriented folding and thrusting that forms sinuous and *en echelon* mountain ranges that are uplifted to the elevations of over 2000 m with the highest peak in the Caribbean islands (Pico Duarte, 3098 m) in the west-central part of the island (Fig. 1). Between these anticlinal, thrust-bounded mountain ranges are synclinal basins that are locally depressed to the elevations of ca. 400 m to more than 30 m below sea level. These basins have received thick deposits of Late Miocene to recent clastic sediments from the erosion of the adjacent anticlinal mountain ranges.

To estimate how active deformation is partitioned in Hispaniola between the two strike-slip faults and the adjacent areas of folds and thrust faults, we calculated geomorphological indices for both river segments (normalized steepness index) and terrain surfaces (surface roughness) that are derived from a digital elevation model (DEM). These geomorphological indices show fundamental variations across Hispaniola. In order to test if the geomorphological variations reflect active tectonic deformations, we constructed regional two-dimensional (2D) forward gravity models along four transects to constrain the crustal thickness variations that may act as the controls on deformation style. We then correlate these crustal structures with thicknesses of clastic sedimentary rocks in the basin areas of Hispaniola to infer optimal areas of petroleum prospectivity.

Data and methods

Geomorphology

Tectonic geomorphology reveals how tectonic processes shape the modern landscape – along with non-tectonic processes that include weathering, sediment transport, and sediment deposition (Mayer 2000). Sediment flux from fluvial streams is a crucial link between tectonics, geomorphology, and atmospheric precipitation. Within each watershed (i.e., an area that channels precipitation to an outflow point), the landscape evolution is controlled by: 1), the incision of the river network into the bedrock (Hovius 2000); 2), by tectonic uplift; and 3) by atmospheric precipitation. The river networks can be extracted from a DEM, assuming that water flows into the neighbouring cell with the highest slope between them (Greenlee 1987; Jenson & Domingue 1988; Tarboton *et al.* 1991). A river profile is also modified by the competing processes of uplift and erosion (Hovius 2000), and typically an equilibrium state is quickly attained along a river channel within tens of thousands years (Begin *et al.* 1981; Snow & Slingerland 1987; Hume & Herdendorf 1988; Roering *et al.* 2001). Actively uplifting orogenic belts produce much steeper river gradients than areas unaffected by tectonics (Merritts *et al.* 1994). For this reason, regional studies of river gradient can provide an indicator for active crustal deformation.

This study uses data from the shuttle radar topography mission (DEM version 3) (Farr *et al.* 2007) to analyse the tectonic geomorphology of Hispaniola. The data has a spatial resolution of 1 arc-second (about 30 meters) and an absolute height error of 8.0 m for islands (Rodríguez *et al.* 2006). The DEM was projected into UTM Zone 19N so that each grid cell has the same geometrical size. We delineated the river network with catchment areas larger than 5 km^2 using the hydrology toolbox in ArcGIS 10.7 (ESRI, Redlands, California, USA). The cut-off at 5 km^2 ensured that we are only studying fluvial processes where rivers incise bedrock (Willgoose *et al.* 1991). We computed the stream orders following Strahler (1957) and delineated watershed boundaries of each fluvial system using river junctions and river mouth as outflow pour-points. Sub-watersheds of low-order rivers are merged into large watersheds of high-order rivers. We constructed a longitudinal profile along each river segment by plotting elevations against distances to the river mouth and calculated the normalized steepness index (k_{sn}) for each stream pixel along the profiles as:

$$\mathrm{k}_{sn} = \frac{Slope}{\mathrm{A}\text{^}(-\theta_{ref})} \quad (1)$$

where *Slope* is the along profile gradient (the ratio of vertical drop to horizontal distance), *A* is the catchment area, and ϑ_{ref} is the reference concavity index that normally uses a value of 0.45 (Wobus *et al.* 2006). Typically, an equilibrium state is maintained, and a concave-up form describes the longitudinal profile of a river. Tectonic, base-level, or lithological perturbations express higher k_{sn} values (Kirby & Whipple 2001). Knickpoints, or abrupt changes in channel elevation or slope, are also extracted from longitudinal profiles to highlight areas of differential active uplift.

Besides the geomorphological indices for rivers, the surface roughness (SR) were calculated for the terranes:

$$SR = \frac{terrane\ surface\ area}{flat\ surface\ area}. \quad (3)$$

This index determines the relative landform age as well as the degree of dissection. SR values vary from 1.0 for young surface lacking incision to 1.2 for older surfaces with substantial incision (Domínguez-González *et al.* 2015).

Structural modelling

Four 2-dimensional (2D) gravity models were constructed, varying in length from 778 km to 1001 km to span the entire deformed zone of the North American-Caribbean plate boundary zone. The objective was to model the deep crustal and lithospheric structures beneath the island of Hispaniola that act as the fundamental controls on the overlay tectonic geomorphology of the island (Fig. 1). Our source for marine gravity anomalies data is satellite-derived free air gravity anomalies (Sandwell *et al.* 2014), and our source for land gravity anomalies is the Decade North American Geology (DNAG) Bouguer gravity anomalies compilation (Committee for the Gravity Anomaly Map of North America 1987) (Fig. 2).

The free-air gravity anomalies have an approximate accuracy of 2 mGal (Sandwell *et al.* 2014), and the estimated accuracy of DNAG Bouguer gravity anomalies varies between 1 to 5 mGal (Tanner *et al.* 1999). For the topography of Hispaniola and its offshore areas, we merged data from the U.S. Geological Survey (USGS) global 30 arc-second elevations (Gtopo30) (USGS Center for Earth Resources Observation and Science 1996) and the world terrain base bathymetry. Gravity anomalies data were sampled from the free air and Bouguer gravity anomaly grids along the four gravity transects for marine and land areas, respectively. We added the discrepancy values between two gravity anomaly sources at marine-land contacts to the marine free-air gravity anomalies so that the extracted gravity anomaly data are continuous and smooth. The air density in the gravity models were set as 2.67 g/cm^3 to compensate for the Bouguer correction on land (Tanner *et al.* 1999). The top of crystalline basement, upper-lower crust transition surface, and Moho surface along the four gravity profiles were constrained from: 1) previous seismic refraction results (Ewing *et al.* 1960; Bunce & Fahlquist 1962; Houtz & Ewing 1964; Bunce *et al.* 1969; Ludwig *et al.* 1975; Houtz & Ludwig 1977); 2), teleseismic receiver function studies (Corbeau *et al.* 2017); and 3) wide-angle seismic studies (Núñez 2014; Núñez *et al.* 2019). For areas where information for the top of the crystalline basement was not available, we created a basement top by subtracting the sediment thickness estimated by Straume et al. (2019) from the topography.

The lithosphere mantle was modelled with a constant density of 3.3 g/cm^3 and the asthenosphere mantle was modelled with a constant density of 3.26 g/cm^3 (Dziewonski & Anderson 1981; Christensen & Mooney 1995). The lithosphere-asthenosphere boundary was estimated to reach 135 km deep under Hispaniola and vary at subduction zones (González *et al.* 2012; Possee *et al.* 2019a). The density of lower crust was set to 2.9 g/cm^3, the density of oceanic upper crust, island arc, and CLIP were all modelled with 2.75 g/cm^3 because their dominant lithology is basalt (Dziewonski & Anderson 1981; Christensen & Mooney 1995). The density of sediments above the crystalline basement was set to 2.35 g/cm^3 for thicker sediments and 2.3 g/cm^3 for thinner sediments. Seawater was modelled with a density of 1.03 g/cm^3.

In order to understand the tectonic processes in the mantle, we plotted earthquake epicentres with magnitudes ≥ 3.5 from the January 1918 to October 2019 within 100-km-wide corridors along our four regional gravity transects (U.S. Geological Survey 2019). We also plotted focal mechanisms for earthquakes with magnitudes ≥ 5.0 occurring between January 1976 and December 2017 from the

Harvard Global Centroid-Moment-Tensor (CMT) Project (Dziewonski *et al.* 1981; Ekström *et al.* 2012).

Results

Geomorphology

Watersheds. The river network and watershed boundaries of Hispaniola are extracted from the topographic DEM (Fig. 3). Two sixth-order watersheds, five fifth-order watersheds, and twenty-two fourth-order watersheds are derived from the stream orders that cover 48 132 km^2 - or about two-thirds of the island (Fig. 3). The two highest-order rivers are the Artinonite River (Haiti) and Rio Ozama (Dominican Republic). The larger river channels on Hispaniola are tectonically controlled by west-northwest and northwest-striking strike-slip and thrust faults (e.g., Artibonite River in watershed “i”, Yaque del Norte in watershed “l”, and Yuna River in watershed “q”; Fig. 3). The Momance River shown in Fig. 3 is offset for about 14.6 km westward by the left-lateral strike-slip EPGFZ (Fleur *et al.* 2019).

River longitudinal profiles as uplift indicators. The longitudinal profiles of 28 river systems and their knickpoints are summarized in Fig. 4. These profiles show general concave-upward trends with local variations. Larger watersheds of higher stream order (Figs. 4i, 4j, 4l-4n, 4q, and 4v) display much more tributary channels than the smaller watersheds. Watersheds in western and central Hispaniola (Figs. 4a - 4u) are often sourced from high elevation (> 2 km) mountain ranges and generally show higher average k_{sn} values and more knickpoints than watersheds in the lower elevation areas of eastern Hispaniola (Figs. 4v - 4ab). Differences in channel slopes are difficult to discern on Fig. 4 because of their different scales, but the k_{sn} values reflect slope variations. Watersheds that include larger proportions of mountainous areas (Figs. 4d - 4f, 4m, 4s, and 4t) show higher average k_{sn} values and contain more knickpoints than watersheds in mostly basin or valley areas. Some fourth-order watersheds in eastern Hispaniola entirely lack knickpoints (Figs. 4x and 4ab).

Normalized steepness index and knickpoints. Along the river network of 7815 segments between tributary channels, the calculated k_{sn} values of river segments range between 0 and 635. Only 1.34% of river segments have k_{sn} values higher than 200, 8.43% of river segments have k_{sn} values higher than 100, and 61.29% of river segments have k_{sn} values less than 30. In basin areas without significant topographic relief, k_{sn} values are generally below 30 and can reach as low as 0, whereas in mountainous areas, k_{sn} values are much higher (Fig. 5). Most of the river segments with high k_{sn} values appear in central and western Hispaniola and are concentrated in specific mountain ranges: Cordillera Central-Massif du Nord, Chaine des Matheux-Sierra de Neiba, and Sierra de Bahoruco-Massif de Selle (Figs. 3 and 5). Across the topographically lower areas of eastern Hispaniola, k_{sn} values rarely reach 60. Extracted knickpoints are also clustered within these mountain ranges in central and western Hispaniola (Fig. 6). Kernel density values - a quantity-per-unit area from point or line features representing the degree of clustering of data - are higher in central and western Hispaniola than in eastern Hispaniola (Fig. 6). These longitudinal profiles and indices indicate that western and central Hispaniola has undergone much greater active uplift than has affected eastern Hispaniola.

Surface Roughness. The terrane geomorphological index SR (Fig. 7) display a similar trend to the stream indices: the higher SR values (≥ 1.05) occur mostly in the mountainous areas of central and western Hispaniola with the highest value reaching 1.24, while most of eastern Hispaniola displays low SR values (≤ 1.04). This SR distribution reveals that central and western Hispaniola have undergone more extensive incision than eastern Hispaniola.

Gravity modelling and interpretation

We plotted earthquakes within 100-km-wide corridors along our gravity transects to understand the crustal structure of Hispaniola and the locations and geometries of subducted slabs beneath the island (Figs. 8-11). Two of the gravity transects cross central and western Hispaniola, and the other two transects cross eastern Hispaniola (Fig. 1). North of Hispaniola, the three western transects (Figs. 8-10) cross the Bahamas and North Hispaniola Trench, and the eastern transect crosses the Puerto Rico Trench. South of Hispaniola, the two eastern transects (Figs. 10 and 11) cross the Muertos Trough.

Forward modelling of calculated gravity anomaly data show good agreement with the measured gravity anomaly data (Figs. 8-11). Free-air gravity lows correlate with deep bathymetric trenches that include the North Hispaniola Trench, Puerto Rico Trench, and Muertos Trough (Figs. 8-11). Some gravity lows are produced by the thickened oceanic crust that underlies the Bahamas and CLIP. Free air gravity highs are often related to high-standing bathymetrical features such as the Bahamas carbonate banks (Figs. 8-10).

Onshore Bouguer gravity anomalies have lower amplitudes than marine free air anomalies and generally mimic the topography of the underlying Moho. The positive anomaly at about 180 km along Transect 1 correlates with an area of elevated Moho observed in the CLIP region south of EPGFZ (Fig. 8). This elevated Moho on Transect 1 is also interpreted on the conceptual transect based on teleseismic receiver functions by Corbeau et al. (2017). However, we do not model an elevated Moho south of EPGFZ on our Transect 2 (Fig. 9) because it is not supported by a positive gravity anomaly.

The Moho surfaces interpreted from wide-angle seismic studies by Nunez (2014) and Nunez et al. (2019) were not included in our Transects 2 and 3 (Figs. 9 and 10) because Moho surfaces at these proposed depths could not be supported by gravity modelling. The Moho surface in our Transect 2 (Figs. 9) is typically 3-8 km deeper than their Moho interpreted at the 6.3-7.6 km/s transition. Also, our Transect 2 Moho is about 6 km shallower than the interpreted Moho at the 7.6-8.0 km/s transition. Our upper-lower crust transition in Transect 2 is roughly consistent with wide-angle seismic studies. The Moho and upper-lower crust transition surface in our Transect 3 show similar trends with Transect 2 when compared with the wide-angle seismic studies. It should be noted that the density structure in this study is a first-order estimation without detailed geological/geophysical constraints, additional density and/or structural control may improve our understanding of inconsistencies between different methods.

Another P-to-S receiver function study (Kumar *et al.* 2020) agreed with wide-angle seismic study (Núñez 2014) on in area of 22-km-thick crust in eastern Hispaniola. Our study is consistent with the 32-38 km crustal thickness in western Dominican Republic (central Hispaniola) from the P-to-S receiver function study (Kumar *et al.* 2020), except for the 21.7 km crustal thickness near EPGFZ.

The crust is thicker beneath central and western Hispaniola (about 33-45 km thick, Figs. 8 and 9) than in eastern Hispaniola (about 29-36 km, Figs. 10 and 11), suggesting that central and western Hispaniola have undergone a larger amount of crustal thickening. The crust beneath the Bahamas Platform is much thicker (15-25 km, Figs. 8-10) than adjacent normal Atlantic oceanic crust (5-7 km) (Figs. 8-11). Our modelled crustal thickness of the Bahamas (15-25 km) is slightly higher than the 15-20 km shipboard gravity thickness from Uchupi et al. (1971) but remains thicker than the normal 5-8-km-thick oceanic crust thickness for the adjacent Atlantic ocean to the east. The crust of the Bahamas may have been thickened in this region as a part of the Central Atlantic Magmatic Province during Triassic time (Dale 2013; Reuber *et al.* 2016).

The CLIP crust is also thicker (normally 6-16 km and reaches 20 km at the Beata Ridge) (Nunez *et al.* 2016) than normal oceanic crust (typically 5-8 km). Our models for the crustal structure of the CLIP provide a reasonable fit between calculated and observed gravity anomalies and show good correspondence with the previous refraction data.

Beneath central and western Hispaniola, there are very few intermediate earthquakes with depths greater than 70 km (1 of 67 earthquakes near Transect 1, Fig. 8 and 11 of 129 earthquakes near Transect2, Fig. 9). Beneath eastern Hispaniola, there is a southwest-dipping zone of intermediate earthquakes (344 of 528 earthquakes near Transect 3, Fig. 10 and 455 of 833 earthquakes near Transect 4, Fig. 11). The maximum earthquake depths reach 96 km near Transect 1 (Fig. 8) and 134 km near Transect 2 (Fig. 9), whereas they reach 209 km near both Transects 3 and 4 (Figs. 10 and 11).

Intermediate depth earthquakes reflect two actively subducting slabs beneath eastern Hispaniola: a subducted North American plate (Atlantic slab) dipping to a depth of 209 km at a steeper 45 ° angle and a subducted Caribbean plate (CLIP slab) extending only 70 km into the uppermost mantle at a very shallow 10 - 20 ° dip angle (Figs. 10 and 11) (Byrne *et al.* 1985; Granja Bruña *et al.* 2010). Transect 4 runs roughly parallel with the SW-NE convergent direction and Transect 3 is instead in S-N direction, so the true dip of the North American plate slab is steeper as seen in Transect 4 (Fig. 11) than the apparent shallower dip seen in Transect 3 (Fig. 10).

Discussion

Inferring areas of active uplift from geomorphology

Higher k_{sn} (Fig. 5) values of the rivers, more clustered knickpoints (Fig. 6), and higher surface roughness (Fig. 7) from central and western Hispaniola reflect more uplift and incision in the topographically-elevated areas of central and western Hispaniola than the topographically lower area of eastern Hispaniola. The uplift and incision may be controlled by more factors other than only by tectonics and crustal shortening; additional factors could include lithological variations along the length of river channels and significant climatic variations on the windward (northeastern) and leeward (southwestern) sides of the mountain ranges of central and western Hispaniola (DiBiase & Whipple 2011; Whittaker 2012; Cyr *et al.* 2014; Kober *et al.* 2015).

Bedrock that is more resistant to physical weathering is assumed to have a lower erosion rate compared to adjacent areas of more erodible bedrock (Tucker 2004). As a basement terrane is uplifted in the core of a mountain range, streams incise more deeply into softer bedrocks and less deeply into harder bedrocks. This pattern of differential erosion leads to higher k_{sn} values in the softer bedrocks and lower k_{sn} values in adjacent channel areas of harder bedrocks (Cyr *et al.* 2014).

For western and central Hispaniola, we observe that k_{sn} values remain remarkably similar regardless of whether the river channel is incising harder metamorphic and volcanic rocks or softer sedimentary lithologies. We also observe that k_{sn} values are similar on either the more humid and windward northeastern side of the Cordillera Central – or the drier and leeward southwestern side "rain shadow" of the range. Because of these two observations - no links between k_{sn} values and either rock hardness or climate - we infer that in this tropical setting, tectonic deformation is the main contributor to the island's geomorphology. Cotilla and Cordoba (2009) reached a similar conclusion in their studies of the transverse asymmetry of valleys and fluvial terraces in central Hispaniola where they showed that rivers in this area are mainly controlled by neotectonic uplift.

A third observation supporting the dominance of tectonics on geomorphology over the factors like rock hardness and climate is the close association of the highest k_{sn} values with Miocene to recent large anticlines and thrust faults in western and central Hispaniola as compiled from Mann et al. (1995) and Secretary of Industry and Commerce (2005) (Fig. 12). The areas of high k_{sn} values parallel the northwest to southeast bands that extend from the Cordillera Central to the southern peninsula of Haiti. Recent studies by Corbeau et al. (2016), Wang et al. (2018), and Possee et al. (2019b) have described geological evidence for Holocene uplift and deformation along these folds and for Holocene displacement along the left-lateral EPGFZ (Fig. 12).

The fold axes and associated thrusts in south-central Hispaniola are also roughly perpendicular to the directions of GPS vectors in this area that are displayed relative to a fixed Caribbean plate (Calais *et al.* 2016; Symithe & Calais 2016; Wang *et al.* 2018) (Fig. 13). The relative velocities near the Septentrional fault zone are much larger than the velocities near the EPGFZ. The relative motion is NEE-SWW with a significant component of left-lateral strike-slip near the Septentrional fault zone. Near the Cordillera Central-Massif du Nord and Chaine des Matheux-Sierra de Neiba mountain ranges, the inter-plate relative motion is NE-SW, roughly perpendicular to the thrust faults, and at a high angle to the left-lateral strike-slip faults like the EPGFZ. Near the Massif de la Hotte on western peninsula north of EPGFZ, the relative motion is roughly E-W showing left-lateral strike-slip with less transpression. These changes in both directions and velocities signify that the crustal shortening is partitioned in the *en echelon* and highly transpressional mountains between the two major strike-slip fault systems in central and western Hispaniola and result in the active uplift described here.

Along-strike variations of the oblique convergence plate boundary zone

Tectonic geomorphology. The east-west variations in geomorphological indices show that central and western Hispaniola are experiencing more active uplift than the eastern Hispaniola (Figs. 5-7). This variation may be related with the transition from an oblique collision of Bahamas with 15-25-km-thick crust with central and western Hispaniola to oblique subduction of normal oceanic crust (5-7 km thick) of North American plate beneath eastern Hispaniola. Calais et al. (2016) attributed the changing style of deformation to the changes in the orientation of the plate boundary faults (e.g., the west-southwest-striking, 8-km-deep Puerto Rico Trench is more transtensional than the more northwest-striking transpressional Septentrional fault zone in northern Hispaniola, Fig. 1).

In addition to the changing plate boundary geometry, another critical factor is the crustal types that are juxtaposed by the plate boundary faults. For example, the thickest area of the Bahamas (about 25 km) is adjacent to the area of highest elevation and highest k_{sn} values of central and western Hispaniola (Figs. 5, 8, and 9) – along with the areas of high surface roughness (Fig. 7).

The boundary between these topographically-elevated areas and the lower area of eastern Hispaniola is shown by the yellow line in maps in Figs. 5-7 and 12-13. This yellow line also marks the eastern tip of the Bahamas Platform and a boundary between the 4-km-deep North Hispaniola Trench and the 8-km-deep Puerto Rico Trench (Rodríguez-Zurrunero *et al.* 2019). This abrupt transition is also apparent from the free-air gravity anomalies which is wide and prominent to the east over the Puerto Rico Trench subduction but less prominent and narrower in the North Hispaniola Trench between the thick crusts of Bahamas and Hispaniola (Fig. 2). The trench is less prominent along the edge of the Bahamas because the thicker crust is being obliquely subducted and filling the trench.

Southward subduction and collision of the North American plate. We interpret that in areas east of the yellow line, the normal-thickness oceanic crust is subducting under Puerto Rico and eastern Hispaniola, and to the west of the yellow line, the thicker Bahamas crust collides with central and western Hispaniola and produces only crustal thickening with no discernible subducted slabs (Transects 1 and 2, Figs. 8 and 9). The boundary-normal, north-south shortening to the east is taken up by the subducting slab (Transects 3 and 4, Figs. 10 and 11).

Supporting evidence beneath eastern Hispaniola includes the presence of intermediate to deep earthquakes in Puerto Rico and eastern Hispaniola that define two Benioff zones (Figs. 10 and 11). The south-dipping Benioff zone beneath eastern Hispaniola is the western extension of the west-dipping Benioff zone beneath the Lesser Antilles island arc (McCann & Sykes 1984; van Benthem *et al.* 2013). The global P-wave UU-P07 tomography imaged a high-velocity anomaly (northern Lesser Antilles) beneath Puerto Rico and Hispaniola which is connected to the subduction of Lesser Antilles (van Benthem *et al.* 2013). These authors also proposed that a southwestward subducted northern Great Arc of Caribbean is present in the mantle at depths of 800-1000 km (van Benthem *et al.* 2013).

Dolan et al. (1998) and Dolan and Wald (1998) attributed a series of large earthquakes in northern Hispaniola during 1946-1953 with oblique, left-lateral thrust motion to the active, oblique collisional underthrusting of Bahamas under Hispaniola. The collision front is the North Hispaniola deformed belt that forms the active boundary between the Silver and Navidad banks (Rodríguez-Zurrunero *et al.* 2019). This collisional zone is characterized by slow velocities at short periods in ambient noise seismic tomography that is consistent with an accretionary complex and supportive of the active Bahamas-Hispaniola collision (Quiros *et al.* 2018).

Dolan et al. (1998) and Dolan and Wald (1998) proposed underthrusting of the Bahamas beneath central and northern Hispaniola – but only to a minimal depth. Symithe and Calias (2016) used earthquake data to highlight a south-dipping slab down to a depth of over 110 km beneath central Hispaniola. Corbeau et al. (2019) proposed that some deep earthquakes with depths larger than 200 km south of EPGFZ and near Jamaica could represent an active or remnant slab of the North American plate subducted southward beneath Hispaniola.

Our compilation of earthquakes from central and western Hispaniola show no evidence for a southward dipping slab of the North American plate (Figs. 8 and 9) yet provide ample evidence for twin subducted slabs beneath eastern Hispaniola (Figs. 10 and 11). On Fig. 14, we compile earthquake focal mechanisms from the Harvard global CMT project (Ekström *et al.* 2012) to show thrust events extending to depths of 110-160 km beneath eastern Hispaniola. This deep thrusting is consistent with the south-dipping Atlantic slab extending southward at least 140 km from North Hispaniola deform belt. The eastern Hispaniola area is characterized by sub-crustal, intermediate to deep earthquakes, while the western Hispaniola area is characterized mainly by shallow, crustal earthquakes.

We propose the possibility of a slab tear in the location of the yellow line shown on Figs. 5-7 and 12-14 that marks the eastern edge of the Bahamas carbonate platform (Rodríguez-Zurrunero *et al.* 2019). This boundary also marks the fundamental change in the tectonic geomorphology of the island, as shown on Figs. 5-7. This slab tear marks the transition from an oblique collision of Bahamas with 15-25-km-thick oceanic crust with the central and western Hispaniola to an oblique subduction of normal oceanic crust (5-7 km thick) of North American plate beneath eastern Hispaniola.

About 350-400 km east of our proposed location of a slab tear, Meighan et al. (2013) proposed that the Benioff zone of the North American plate exhibits a sudden dip change at 64.5 °W reflecting a slab tear and has produced two earthquake swamps. The Lesser Antilles slab to the east has a gentler dip, while the Puerto Rico slab to the west has a steeper dip (Meighan *et al.* 2013). Our proposed similar tear may be present beneath central Hispaniola and deserves further study. One possible manifestation of a slab tear are alkali, mantle-derived volcanic rocks aligned in the northeast trends in this area (Wadge & Wooden 1982)

Northward subduction of the Caribbean plate. Gravity Transects 3 and 4 (Figs. 10 and 11) show the presence of a northward dipping Caribbean slab extending a low dip of ~20 ° for a distance of at least 150 km beneath eastern Hispaniola. Previous workers have proposed a short, 10-15 ° northward-dipping 70-km-long Benioff zone (Byrne *et al.* 1985; Dillon *et al.* 1994; Dolan *et al.* 1998; Mann *et al.* 2002) that resembles the low-angle and amagmatic style of CLIP subduction beneath northern Colombia (Bernal-Olaya *et al.* 2015). Dolan et al. (1998) proposed that the two slabs intersect at depth and that the shallower-dipping Caribbean slab may have driven the North American slab to its steeper dip.

GPS data show very slow (less than 2 mm/year) convergence at the Muertos Trough (Symithe & Calais 2016), possibly due to the impedance of the North American slab. Other groups have proposed that there is no “true subduction” but is instead “distributed thrusting” in the lower crust (ten Brink *et al.* 2009; Granja Bruña *et al.* 2010). Ten Brink et al. (2009) and Granja Bruña et al. (2010) concluded that the 1984 thrust earthquakes ranging in depth from 16 to 33 km (Fig. 14) reflect crustal deformation and disagreed with Byrne et al. (1985) that these events were related to low-angle slab subduction along the Muertos Trough. This interpretation seems unlikely as we see three mantle earthquakes with thrust focal mechanisms and magnitudes of 6.65, 6.19, and 5.44 occurred in 1979 and 2010 (Ekström *et al.* 2012) beneath eastern Hispaniola at depths of about 80 km (Fig. 14). This is consistent with our proposal for an active slab extending at least 80 km to the north from the Muertos Trough. Moreover, these mantle earthquakes are too shallow to be attributed to the North American subducted slab at these locations (all would need to be at least 120-150 km deep to be part of the North American plate). The global P-wave UU-P07 tomography also shows the Muertos high-velocity anomaly consistent with a Muertos subducted slab of the inferred length (van Benthem *et al.* 2013).

Application of this study for petroleum prospectivity in Hispaniola and Puerto Rico

Tillman and Mann (this volume) compiled the sedimentary thickness from 2D seismic reflection lines in the onshore basins between mountain ranges (Cibao Basin, San Juan Basin, Enriquillo Basin, Azua Basin) and in offshore basins around Hispaniola (Fig. 15). The area of greatest sedimentary thickness in the range of 3 to 6 km is concentrated in thrust-bounded, synclinal "ramp" basins of central and western Hispaniola (Mann *et al.* 1991a). The thickest of these basins are the Cibao Basin in the northern Hispaniola (3-6 km), the plateau Central-San Juan-Azua basins of central Hispaniola (3-5.5 km), and the Cul-de-Sac-Enriquillo basin of southern Hispaniola (3-5 km).

These three onshore basins are visible in our Transects 1 and 2 (Figs. 8 and 9) and can be related to the large scale folding of the island arc crust beneath central and western Hispaniola. As these deeper basins are bounded by thrust faults on both sides, they dynamically depress the intervening synclinal block and produce accommodation space that is filled by the erosion of both of the adjacent and actively uplifting, anticlinal mountain blocks (Mann *et al.* 1991a). On the other hand, basins on the flanks of the central basement high of eastern Hispaniola and Puerto Rico are less faulted and have a uniformly thin, clastic sedimentary cover (Fig. 15).

As summarized by Tillman and Mann (this volume), all of the natural oil and gas seeps in Hispaniola are associated with either the plateau Central-San Juan-Azua and Cul-de-Sac-Enriquillo basins. Maturity studies show that both have entered or close to the oil window based on existing geochemical data and assuming a Middle Miocene carbonate source rock.

Outside of the area of central and western Hispaniola, the sedimentary thickness is more uniform, less fault-controlled, and rarely exceeds 3 km in thickness. These areas lack thick sedimentary sections and also are not associated with natural oil and gas seeps and therefore are less prospective than the Plateau Central-San Juan-Azua trend.

Conclusion

Normalized steepness indices and surface roughness were calculated for the 72 284 km^2 island of Hispaniola to reveal areas of more active uplift in the topographically-elevated areas of central and western Hispaniola and less active uplift in the less elevated area of eastern Hispaniola (Figs. 5 and 7). Areas of higher uplift in central and western Hispaniola are spatially associated with the axes of northwest-striking *en echelon* fold axes (Fig. 12).

Four regional 2D gravity transects ranging in length from 778 km to 1001 km (Figs. 8-11) were constructed to constrain the crustal structure that underlie the distinctly different topographic areas of western and central versus eastern Hispaniola. Four gravity transects show that the collisional zone in Hispaniola is formed by the oblique juxtaposition of four crustal types: 1) 29-45-km-thick, arc crust in Hispaniola; 2) 15-25-km-thick oceanic crust beneath the Bahamas Platform north of Hispaniola; 3) 5-8-km-thick oceanic crust northeast of Hispaniola; and 4) 6-16-km-thick CLIP south of Hispaniola. Intermediate to deep earthquakes beneath eastern Hispaniola indicate active southwestward subduction of normal Atlantic oceanic crust along the North Hispaniola deformed belt and northward subduction of the CLIP along the Muertos Trough.

Integration of the gravity transects with earthquake epicentres reveals that oblique collision in central and western Hispaniola is accommodated by active uplift and crustal shortening with an apparent absence of subducted slabs beneath the western part of the island. We infer that thicker crust of the Bahamas to the north and the CLIP to the south are obliquely converging on the area of island arc crust in central Hispaniola that is shortening, thickening, and being deformed by strike-slip faults. Basin formation in this tectonic environment consists of thrust-bounded, synclinal “ramp” basins filled with clastic rocks of Late Miocent to recent age that have been eroded from the adjacent anticlinal mountain ranges.

Integration of the gravity transects with earthquakes for eastern Hispaniola shows that oblique convergence in this less elevated region is accommodated by negligible crustal shortening and the presence of intermediate to deep earthquakes showing that twin subducted slabs are present beneath the island. We infer that the thinner (5-7 km) oceanic crust east of the Bahamas subducts to the southwest and thicker (6-16) km CLIP crust underlying the Venezuelan basin on the Caribbean plate subducts to the northeast with the area of island arc along the central Hispaniola crust being elevated as a broad arch that lacks significant fault-related basement relief. Basin formation in this tectonic environment mainly consists of offshore forearc basins that accumulate clastic deposits eroded from the uplifted land areas. This same twin subduction environment - that includes the broad basement arch between the two subduction zones - extends to the east and includes the island of Puerto Rico.

Hydrocarbon prospectivity of Hispaniola and Puerto Rico is confined to the deeper, synclinal “ramp” basins of central and western Hispaniola as these basins provide the thickest, late Miocene to recent overburden (3-6 km) in the region (Fig. 15). Rock maturity studies (Tillman and Mann, this volume) show that source rocks of this region are mature or near-to mature and can explain the presence of natural oil seeps and limited historical oil production in this region.

Acknowledgements

We thank Diana Nunez and Ian Davison for their constructive reviews of this paper and we thank Jonny Wu, Songqiao Wei, Sean Romito, Mei Liu, and Muhammad Nawaz Bugti for their suggestions. Special thanks go to Jordane Corbeau for providing us with the Haitian seismic station locations that were used in gravity modelling. We thank Seequent Ltd. for providing the Geosoft Oasis Montaj software and the industry sponsors of the Conjugate Basins, Tectonics, and Hydrocarbons consortium at University of Houston for their continued financial support.

References

Begin, Z.B., Meyer, D.F. & Schumm, S.A. 1981. Development of longitudinal profiles of alluvial channels in response to base-level lowering. *Earth Surface Processes and Landforms*, **6**, 49–68, https://doi.org/10.1002/esp.3290060106.

Benford, B., Demets, C. & Calais, E. 2012. GPS estimates of microplate motions, northern Caribbean: Evidence for a Hispaniola microplate and implications for earthquake hazard. *Geophysical Journal International*, **191**, 481–490, https://doi.org/10.1111/j.1365-246X.2012.05662.x.

Bernal-Olaya, R., Sanchez, J., Mann, P. & Murphy, M. 2015. Along-strike Crustal Thickness Variations of Subducting Caribbean Plate Produces Two Distinctive Styles of Thrusting in the Offshore South Caribbean Deformed Belt, Colombia. *AAPG Memoir*, **108**, 295–332.

Bowin, C. 1975. The Geology of Hispaniola. *In*: *The Gulf of Mexico and the Caribbean*. Springer US, 501–552., https://doi.org/10.1007/978-1-4684-8535-6_12.

Bunce, E.T. & Fahlquist, D.A. 1962. Geophysical investigation of the Puerto Rico trench and outer ridge. *Journal of Geophysical Research*, **67**, 3955–3972, https://doi.org/10.1029/jz067i010p03955.

Bunce, E.T., Fahlquist, D.A. & Clough, J.W. 1969. Seismic refraction and reflection measurements-Puerto Rico outer ridge. *Journal of Geophysical Research*, **74**, 3082–3094, https://doi.org/10.1029/JB074i012p03082.

Byrne, D.B., Suarez, G. & McCann, W.R. 1985. Muertos Trough subduction - microplate tectonics in the northern Caribbean ? *Nature*, **317**, 420–421.

Calais, É., Symithe, S., Mercier de Lépinay, B. & Prépetit, C. 2016. Plate boundary segmentation in the northeastern Caribbean from geodetic measurements and Neogene geological observations. *Comptes Rendus Geoscience*, **348**, 42–51, https://doi.org/10.1016/j.crte.2015.10.007.

Christensen, N.I. & Mooney, W.D. 1995. Seismic velocity structure and composition of the continental crust: A global view. *Journal of Geophysical Research*, **100**, 9761–9788.

Committee for the Gravity Anomaly Map of North America. 1987. *Gravity Anomaly Map of North America*. Boulder, Colorado, Geological Society of America.

Corbeau, J., Rolandone, F., Leroy, S., Mercier de Lepinay, B., Ellouz-Zimmermann, N. & Momplaisir, R. 2016. How transpressive is the northern Caribbean plate boundary? *Tectonics*, **35**, 1032–1046, https://doi.org/10.1002/2015TC003996.

Corbeau, J., Rolandone, F., et al. 2017. Crustal structure of western Hispaniola (Haiti) from a teleseismic receiver function study. *Tectonophysics*, **709**, 9–19, https://doi.org/10.1016/j.tecto.2017.04.029.

Corbeau, J., Gonzalez, O.L., et al. 2019. Is the local seismicity in western Hispaniola (Haiti) capable of imaging northern Caribbean subduction? *Geosphere*, **15**, 1–13, https://doi.org/10.1130/ges02083.1.

Cotilla Rodriguez, M.O. & Cordoba Barba, D. 2009. The hispaniola fluvial system and its morphostructural context. *Physical Geography*, **30**, 453–478, https://doi.org/10.2747/0272-3646.30.5.453.

Cyr, A.J., Granger, D.E., Olivetti, V. & Molin, P. 2014. Distinguishing between tectonic and lithologic controls on bedrock channel longitudinal profiles using cosmogenic 10Be erosion rates and channel steepness index. *Geomorphology*, **209**, 27–38, https://doi.org/10.1016/j.geomorph.2013.12.010.

Dale, A.J. 2013. *Crustal Type, Tectonic Origin, and Petroleum Potential of the Bahamas Carbonate*

Platform. University of Houston.

DiBiase, R.A. & Whipple, K.X. 2011. The influence of erosion thresholds and runoff variability on the relationships among topography, climate, and erosion rate. *Journal of Geophysical Research: Earth Surface*, **116**, 1–17, https://doi.org/10.1029/2011JF002095.

Diebold, J., Driscoll, N., EW-9501-Science Team & Hsu, K.J. 1999. New insights on the formation of the Caribbean basalt province revealed by multichannel seismic images of volcanic structures in the Venezuelan Basin. *In*: Mann, P. (ed.) *Caribbean Basins*. Amsterdam, The Netherlands, Elsevier Science B.V., 561–589.

Dillon, W.P., Edgar, N.T., Scanlon, K.M. & Coleman, D.F. 1994. A review of the tectonic problems of the strike-slip northern boundary of the Caribbean Plate and examination by GLORIA. *In*: Gardner, J. V., Field, M. E. & Twichell, D. C. (eds) *Geology of the United States' Seafloor: The View from Gloria*. Cambridge University Press, 135–164.

Dolan, J.F. & Wald, D.J. 1998. The 1943-1953 north-central Caribbean earthquakes: Active tectonic setting, seismic hazards, and implications for Caribbean-North American plate motions. *In*: Dolan, J. F. & Mann, P. (eds) *Active Strike-Slip and Collisional Tectonics of the Northern Caribbean Plate Boundary Zone*. Boulder, CO, Geological Society of America, 143–169.

Dolan, J.F., Mullins, H.T. & Wald, D.J. 1998. Active tectonics of the north-central Caribbean: Oblique collision, strain partitiohning, and opposing subducted slabs. *In*: Dolan, J. F. & Mann, P. (eds) *Active Strike-Slip and Collisional Tectonics of the Northern Caribbean Plate Boundary Zone*. Boulder, CO, Geological Society of America, 1–61.

Domínguez-González, L., Andreani, L., Stanek, K.P. & Gloaguen, R. 2015. Geomorpho-tectonic evolution of the jamaican restraining bend. *Geomorphology*, **228**, 320–334, https://doi.org/10.1016/j.geomorph.2014.09.019.

Dziewonski, A.M. & Anderson, D.L. 1981. Preliminary reference Earth model. *Physics of the Earth and Planetary Interiors*, **25**, 297–356, https://doi.org/10.1016/0031-9201(81)90046-7.

Dziewonski, A.M., Chou, T.-A. & Woodhouse, J.H. 1981. Determination of earthquake source parameters from waveform data for studies of global and regional seismicity. *Journal of Geophysical Research*, **86**, 2825–2852, https://doi.org/10.1029/JB086iB04p02825.

Ekström, G., Nettles, M. & Dziewoński, A.M. 2012. The global CMT project 2004-2010: Centroid-moment tensors for 13,017 earthquakes. *Physics of the Earth and Planetary Interiors*, **200–201**, 1–9, https://doi.org/10.1016/j.pepi.2012.04.002.

Ewing, J.I., Antoine, J. & Ewing, M. 1960. Geophysical measurements in the western Caribbean and Gulf of Mexico. *JOURNAL OF GEOPHYSICAL RESEARCH*, **65**, 4087–4126.

Farr, T.G., Rosen, P.A., et al. 2007. The shuttle radar topography mission. *Reviews of Geophysics*, **45**, Paper number 2005RG000183, https://doi.org/10.1029/2005RG000183.

Fleur, N. Saint, Feuillet, N. & Klinger, Y. 2019. Active tectonics along the Cul-de-Sac – Enriquillo plain and seismic hazard for Port-au-Prince, Haiti. *Tectonophysics*, **771**, 228235, https://doi.org/10.1016/j.tecto.2019.228235.

González, O.F., Alvarez, J.L., Moreno, B. & Panza, G.F. 2012. S-Wave Velocities of the Lithosphere–Asthenosphere System in the Caribbean Region. *Pure and Applied Geophysics*, **169**, 101–122, https://doi.org/10.1007/s00024-011-0321-3.

Granja Bruña, J.L., Muñoz-Martín, A., et al. 2010. Gravity modeling of the Muertos Trough and tectonic implications (north-eastern Caribbean). *Marine Geophysical Research*, **31**, 263–283, https://doi.org/10.1007/s11001-010-9107-8.

Greenlee, D.D. 1987. Raster and Vector Processing for scanned Linework. *Photogrammetric Engineering and Remote Sensing*, **53**, 1383–1387.

Houtz, R.E. & Ewing, J.I. 1964. Sedimentary Velocities of the Western North Atlantic Margin. *Bulletin of the Seismological Society of America*, **54**, 867–895.

Houtz, R.E. & Ludwig, W.J. 1977. Structure of Colombia Basin, Caribbean Sea, from profiler-sonobuoy measurements. *Journal of Geophysical Research*, **82**, 4861–4867, https://doi.org/10.1029/JB082i030p04861.

Hovius, N. 2000. Macroscale process systems of mountain belt erosion. *In*: Summerfield, M. A. (ed.) *Geomorphology and Global Tectonics*. Chichester, UK, John Wiley and Sons, 77–105.

Hume, T.M. & Herdendorf, C.E. 1988. A geomorphic classification of estuaries and its application to coastal resource management-A New Zealand example. *Ocean and Shoreline Management*, **11**, 249–274, https://doi.org/10.1016/0951-8312(88)90022-7.

Jenson, S.K. & Domingue, J.O. 1988. Extracting topographic structure from digital elevation data for geographic information system analysis. *Photogrammetric Engineering and Remote Sensing*, **54**, 1593–1600.

Kirby, E. & Whipple, K. 2001. Quantifying differential rock-uplift rates via stream profile analysis. *Geology*, **29**, 415–418, https://doi.org/10.1130/0091-7613(2001)029<0415:QDRURV>2.0.CO;2.

Kober, F., Zeilinger, G., et al. 2015. Tectonic and lithological controls on denudation rates in the central Bolivian Andes. *Tectonophysics*, **657**, 230–244, https://doi.org/10.1016/j.tecto.2015.06.037.

Kumar, S., Agrawal, M., Pulliam, J., Rivera, E.P. & Huérfano, V.A. 2020. Crustal thickness and bulk Poisson ratios in the Dominican Republic from receiver function analysis. *Tectonophysics*, **775**, 228308, https://doi.org/10.1016/j.tecto.2019.228308.

Leroy, S., Ellouz-Zimmermann, N., et al. 2015. Segmentation and kinematics of the North America-Caribbean plate boundary offshore Hispaniola. *Terra Nova*, **27**, 467–478, https://doi.org/10.1111/ter.12181.

Ludwig, W., Houtz, R. & Ewing, J. 1975. Profile-sonobuoy measurements in the Colombian and Venezuelan Basins, Caribbean Sea. *American Association of Petroleum Geologists Bulletin*, **59**, 115–123.

Mann, P., Burke, K. & Matumoto, T. 1984. Neotectonics of Hispaniola: plate motion, sedimentation, and seismicity at a restraining bend. *Earth and Planetary Science Letters*, **70**, 311–324, https://doi.org/10.1016/0012-821X(84)90016-5.

Mann, P., Draper, G. & Lewis, J.F. 1991a. *An Overview of the Geologic and Tectonic Development of Hispaniola*.

Mann, P., Tyburski, S.A. & Rosencrantz, E. 1991b. Neogene development of the Swan Islands restraining-bend complex, Caribbean Sea. *Geology*, **19**, https://doi.org/10.1130/0091-7613(1991)019<0823:NDOTSI>2.3.CO;2.

Mann, P., Lebron, M.C., Rodriguez, J. & Heubeck, C. 1995. Geologic map of the Dominican Republic. *In*: Mann, P., Draper, G. & Lewis, J. F. (eds) *Geologic and Tectonic Development of the North America-Caribbean Plate Boundary in Hispaniola: Geological Society of America Special Paper 262*. Geological Scoiety of America.

Mann, P., Calais, E., Ruegg, J.-C., DeMets, C., Jansma, P.E. & Mattioli, G.S. 2002. Oblique collision in the northeastern Caribbean from GPS measurements and geological observations. *Tectonics*, **21**, https://doi.org/10.1029/2001TC001304.

Masson, D.G. & Scanlon, K.M. 1991. The neotectonic setting of Puerto Rico. *Geological Society of America Bulletin*, **103**, 144–154.

Mauffret, A., Mercier de Lepinay, B., et al. 1994. Seismic imagery of intraplate transpressive tectonics in the Caribbean oceanic plateau and oceanic crust, Cayman Trough, Aruba Gap: Preliminary results the CASIS Cruise (Images sismiques d'une tectonique transpressive intra-plaque oceanique caraibe (foss. *Comptes Rendus de l'Academie des Sciences, Serie II*, **318**, 1379–1386.

Mayer, L. 2000. Application of digital elevation models to macroscale tectonic geomorphology. *In*: Summerfield, M. A. (ed.) *Geomorphology and Global Tectonics*. Chichester, UK, John Wiley & Sons, 15–27.

McCann, W. & Sykes, L. 1984. Subduction of aseismic ridges beneath the Caribbean plate: Implications for the tectonics and seismic potential of the northeastern Caribbean. *Journal of Geophysical Research*, **89**, 27.

Meighan, H.E., Pulliam, J., ten Brink, U. & López-Venegas, A.M. 2013. Seismic evidence for a slab tear at the Puerto Rico Trench. *Journal of Geophysical Research: Solid Earth*, **118**, 1–9, https://doi.org/10.1002/jgrb.50227.

Merritts, D.J., Vincent, K.R. & Wohl, E.E. 1994. Long river profiles, tectonism, and eustasy: A guide to interpreting fluvial terraces. *Journal of Geophysical Research*, **99**, 14031–14050.

Nunez, D., Cordoba, D., Cotilla, M.O. & Pazos, A. 2016. Modeling the Crust and Upper Mantle in Northern Beata Ridge (CARIBE NORTE Project). *Pure and Applied Geophysics*, **173**, 1639–1661.

Núñez, D. 2014. *Seismic Sturcture of the Crust across NE Caribbean Plate (Dominican Republic)*. PhD Dissertation, Universidad Complutense de Madrid, 317 pp.

Núñez, D., Córdobab, D. & Kissling, E. 2019. Seismic structure of the crust in the western Dominican Republic. *Tectonophysics*, **773**, Article 228224, https://doi.org/10.1016/j.tecto.2019.228224.

Possee, D., Rychert, C., Harmon, N. & Keir, D. 2019a. Imaging Seismic Discontinuities Beneath the North American-Caribbean Plate Boundary Using S-to-P Receiver Functions. *In*: *AGU Fall Meeting 2019*. T23A-04.

Possee, D., Keir, D., et al. 2019b. The Tectonics and Active Faulting of Haiti from Seismicity and Tomography. *Tectonics*, **38**, 1138–1155, https://doi.org/10.1029/2018TC005364.

Prentice, C.S., Mann, P., Taylor, F.W., Burr, G. & Valastro, S. 1993. Paleoseismicity of the North American-Caribbean plate boundary (Septentrional Fault), Dominican Republic. *GEOLOGY*, **21**, 49–52.

Quiros, D.A., Pulliam, J., Barman, D., Polanco Rivera, E. & Huerfano, V. 2018. Ambient Noise Tomography Images Accreted Terranes and Igneous Provinces in Hispaniola and Puerto Rico.

GEOPHYSICAL RESEARCH LETTERS, **45**, 12293–12301, https://doi.org/10.1029/2018GL080095.

Reuber, K.R., Pindell, J. & Horn, B.W. 2016. Demerara Rise, offshore Suriname: Magma-rich segment of the Central Atlantic Ocean, and conjugate to the Bahamas hot spot. *Interpretation*, **4**, T141–T155, https://doi.org/10.1190/int-2014-0246.1.

Rodríguez-Zurrunero, A., Granja-Bruña, J.L., et al. 2019. Submarine morpho-structure and active processes along the North American-Caribbean plate boundary (Dominican Republic sector). *Marine Geology*, **407**, 121–147, https://doi.org/10.1016/j.margeo.2018.10.010.

Rodríguez, E., Morris, C.S. & Belz, J.E. 2006. A global assessment of the SRTM performance. *Photogrammetric Engineering and Remote Sensing*, **72**, 249–260, https://doi.org/10.14358/PERS.72.3.249.

Roering, J.J., Kirchner, J.W. & Dietrich, W.E. 2001. Hillslope evolution by nonlinear, slope-dependent transport: Steady state morphology and equilibrium adjustment timescales. *Journal of Geophysical Research: Solid Earth*, **106**, 16499–16513, https://doi.org/10.1029/2001jb000323.

Sandwell, D.T., Müller, R.D., Smith, W.H.F., Garcia, E. & Francis, R. 2014. New global marine gravity model from CryoSat-2 and Jason-1 reveals buried tectonic structure. *Science*, **346**, 65–67, https://doi.org/10.1126/science.1258213.

Secretary of Industry and Commerce. 2005. *Geological Map of the Dominican Republic 1:250,000*. Mollat, H., Wagner, B. M., Cepek, P. & Weiss, W. (eds).

Snow, R.. S. & Slingerland, R.L.. 1987. Mathematical Modeling of Graded River Profiles. *Journal of Geology*, **95**, 15–33.

Strahler, A.N. 1957. Quantitative analysis of watershed geomorphology. *Transactions, American Geophysical Union*, **38**, 913–920.

Straume, E.O., Gaina, C., et al. 2019. GlobSed: Updated Total Sediment Thickness in the World's Oceans. *Geochemistry, Geophysics, Geosystems*, **20**, 1756–1772, https://doi.org/10.1029/2018GC008115.

Symithe, S. & Calais, E. 2016. Present-day shortening in Southern Haiti from GPS measurements and implications for seismic hazard. *Tectonophysics*, **679**, 117–124, https://doi.org/10.1016/j.tecto.2016.04.034.

Tanner, J.G., Aiken, C.L.V., et al. 1999. *DNAG Gravity Data*.

Tarboton, D.G., Bras, R.L. & Rodriguez-Iturbe, I. 1991. On the extraction of channel networks from digital elevation data. *Hydrological Processes*, **5**, 81–100, https://doi.org/10.1002/hyp.3360050107.

ten Brink, U.S., Marshak, S. & Granja Bruña, J.L. 2009. Bivergent thrust wedges surrounding oceanic island arcs: Insight from observations and sandbox models of the northeastern caribbean plate. *Bulletin of the Geological Society of America*, **121**, 1522–1536, https://doi.org/10.1130/B26512.1.

Tucker, G.E. 2004. Drainage basin sensitivity to tectonic and climatic forcing: Implications of a stochastic model for the role of entrainment and erosion thresholds. *Earth Surface Processes and Landforms*, **29**, 185–205, https://doi.org/10.1002/esp.1020.

U.S. Geological Survey. 2019. ANSS Comprehensive Earthquake Catalog (ComCat)

Documentationhttps://earthquake.usgs.gov/data/comcat.

Uchupi, E., Milliman, J.D., Luyendyk, B.P., Bowin, C.O. & Emery, K.O. 1971. Structure and origin of southern Bahamas. *American Association of Petroleum Geologists Bulletin*, **55**, 687–704.

USGS Center for Earth Resources Observation and Science. 1996. *USGS EROS Archive - Digital Elevation - Global 30 Arc-Second Elevation (GTOPO30)*, https://doi.org/10.5066/F7DF6PQS.

van Benthem, S., Govers, R., Spakman, W. & Wortel, R. 2013. Tectonic evolution and mantle structure of the Caribbean. *Journal of Geophysical Research: Solid Earth*, **118**, 1–18, https://doi.org/10.1002/jgrb.50235.

Wadge, G. & Wooden, J.L. 1982. Late Cenozoic alkaline volcanism in the northwestern Caribbean: Tectonic setting and Sr isotopic characteristics. *Earth and Planetary Science Letters*, **57**, 35–46.

Wang, J., Mann, P. & Stewart, R.R. 2018. Late Holocene Structural Style and Seismicity of Highly Transpressional Faults in Southern Haiti. *Tectonics*, **37**, 3834–3852, https://doi.org/10.1029/2017TC004920.

Whittaker, A.C. 2012. How do landscapes record tectonics and climate? *Lithosphere*, **4**, 160–164, https://doi.org/10.1130/RF.L003.1.

Willgoose, G., Bras, R.L. & Rodriguez-Iturbe, I. 1991. A physical explanation of an observed link area-slope relationship. *Water Resources Research*, **27**, 1697–1702, https://doi.org/10.1029/91WR00937.

Wobus, C., Whipple, K.X., et al. 2006. Tectonics from topography: Procedures, promise, and pitfalls. *Geological Society of America*, **398**, 55–74.

Figure captions

Fig. 1. Topography and bathymetry of the Greater Antilles (Cuba, Jamaica, Hispaniola, Puerto Rico) in the northern Caribbean and the adjacent eastern Bahamas Platform. The island of Hispaniola is shared by Haiti (western third of the island) and the Dominican Republic (eastern two thirds). Major North American-Caribbean plate boundary faults are shown in black and actively deforming microplates are labelled. The oblique convergence direction between North American-Caribbean plates known from GPS geodesy is shown by the large black arrow. Four 2D gravity transects described in this paper are shown as red lines. The seismic refraction/receiver stations used to constrain the gravity models are shown as yellow dots. HM, Hispaniola microplate; NHM, North Hispaniola microplate; PRVIM, Puerto Rico and Virgin Islands microplate; EPGFZ, Enriquillo-Plantain Garden fault zone; OFZ, Oriente fault zone; SFZ, Septentrional fault zone.

Fig. 2. a) DNAG gravity anomalies that display Bouguer gravity anomalies for on land areas and free air gravity anomalies for marine areas (Tanner *et al.* 1999); b) satellite free air gravity anomalies for both on land and marine areas (Sandwell *et al.* 2014).

Fig. 3. Major, known or inferred, active faults of Hispaniola shown as black lines and the river network shown as blue lines along with 29 outlined watersheds of at least fourth order. The relative widths of rivers reflect their calculated flow rates assuming an evenly distributed rainfall onto each grid cell. Sixth-order watersheds are shown in green, fifth-order watersheds are shown in yellow,

and fourth-order watersheds are shown in magenta. Mountain ranges are shaded in light green colour. The oblique convergence direction between North American-Caribbean plates is shown by the large black arrow. The Momance River of southern Haiti is labelled on the map and discussed in the text. The 28 red-coloured watershed letters (a-ab) are keyed to the lettered (28 out of 29) watersheds and their longitudinal profiles shown on **Fig. 4**. CC, Cordillera Central; CM, Chaine des Matheux; CS, Cordillera Septentrional; MH, Massif de la Hotte; MN, Massif du Nord; MS, Massif de Selle; PN, Presqu'ile du Nord-Ouest; SB, Sierra de Bahoruco; SN, Sierra de Neiba; EPGFZ, Enriquillo-Plantain Garden fault zone.

Fig. 4. Longitudinal profiles of river systems within 28 watersheds of Hispaniola shown in map view on **Fig. 3**. Each sub-figure corresponds to a watershed with the same label shown on **Fig. 3**. Both the horizontal and vertical scales are variable. Magenta points indicate convex knickpoints on the longitudinal river profiles. The eastern-most watershed in the Dominican Republic is not included in this compilation because of its small size. Red lines show the longest rivers and blue lines show the main river of the watershed at its highest elevation. Convex knickpoints within fifth- and sixth-order watersheds are not shown because there are too many knickpoints to be visible on this figure. Average k_{sn} values of stream pixels within watersheds are labelled.

Fig. 5. Normalized steepness index (k_{sn}) along the rivers of Hispaniola. The index values are grouped with blue and cyan colours showing lower k_{sn} values and red and yellow colours showing higher k_{sn} values. The oblique convergence direction between North American-Caribbean plates is shown by the large black arrow. The thick yellow line separates the topographically-low eastern Hispaniola area (eastern Dominican Republic) from the topographically-elevated western Hispaniola area (western Dominican Republic and Haiti).

Fig. 6. Knickpoints along Hispaniola rivers are shown as magenta points. The kernel density of the knickpoints is shown by the light to deep blue contouring and deeper blue colour indicates a higher degree of clustering. The oblique convergence direction between North American-Caribbean plates is shown by the large black arrow. The thick yellow line separates the topographically-low eastern Hispaniola area from the topographically-elevated western Hispaniola area.

Fig. 7. Surface roughness (SR) of Hispaniola with green colours showing lower SR values and red and orange-red colours showing higher SR values. The oblique convergence direction between North American-Caribbean plates is shown by the large black arrow. The thick yellow line separates the topographically-low eastern Hispaniola area from the topographically-elevated western Hispaniola area.

Fig. 8. South-north oriented, Gravity Transect 1 across the eastern Bahamas and western Hispaniola (Haiti). Location of this transect is shown on the map in **Fig. 1**. Calculated Bouguer gravity anomalies (thin solid line) are tied to the observed gravity anomalies (thick dashed line) at station 36E (Ewing *et al.* 1960) with the residuals shown as the red line. Crustal surfaces were constrained by seismic refraction stations (Ewing *et al.* 1960; Houtz & Ewing 1964) and teleseismic receiver function stations (Corbeau *et al.* 2017) shown by "x". Black dots represent earthquake epicentres with the sizes of the dots indicating the relative magnitudes of the earthquakes. The short vertical lines through the epicentres indicate the available depth errors for the earthquakes. Coloured layers in the crust and mantle correspond to different densities used for the gravity modelling. EB, Enriquillo

Basin; SJB, San Juan Basin; CB, Cibao Basin; NHT, North Hispaniola Trench; EPGFZ, Enriquillo-Plantain Garden fault zone; SFZ, Septentrional fault zone.

Fig. 9. Southwest-northeast oriented, Gravity Transect 2 across the eastern Bahamas and central Hispaniola (the Dominican Republic). Location of the transect is shown on the map in **Fig. 1**. Calculated Bouguer gravity anomalies (thin solid line) are tied to the observed gravity anomalies (thick dashed line) at station 22C20 (Houtz & Ludwig 1977) with the residuals shown as the red line. Crustal surfaces were constrained by seismic refraction stations shown by “x” (Houtz & Ewing 1964; Houtz & Ludwig 1977) and by a wide angle seismic reflection profile (Núñez *et al.* 2019). Black dots represent earthquake epicentres with the sizes of the dots indicating the relative magnitudes of the earthquakes. The short vertical lines through the epicentres indicate the available depth errors for the earthquakes. Coloured layers in the crust and mantle correspond to different densities used for the gravity modelling. EB, Enriquillo Basin; SJB, San Juan Basin; CB, Cibao Basin; NHT, North Hispaniola Trench; MB, Mouchoir Bank; SB, Silver Bank; EPGFZ, Enriquillo-Plantain Garden fault zone; SFZ, Septentrional fault zone.

Fig. 10. South-north oriented, Gravity Transect 3 across the easternmost Bahamas and eastern Hispaniola (Dominican Republic). Location of the transect is shown on the map in **Fig. 1**. Calculated Bouguer gravity anomalies (thin solid line) are tied to the observed gravity anomalies (thick dashed line) at station 5E (Houtz & Ewing 1964) with the residuals shown in the red line. Crustal surfaces were constrained by seismic refraction stations shown by “x” (Houtz & Ewing 1964; Ludwig *et al.* 1975) and by wide angle seismic reflection profiles (Núñez 2014). This transect crosses Transect 4 (also shown by “x”). Black dots represent earthquake epicentres with the sizes of the dots indicating the relative magnitudes of the earthquakes. The short vertical lines through the epicentres indicate the available depth errors for the earthquakes. Coloured layers in the crust and mantle correspond to different densities used for the gravity modelling. MT, Muertos Trough; NHT, North Hispaniola Trench; NBP, Navidad Bank Passage.

Fig. 11. Southwest-northeast oriented, Gravity Transect 4 across the Puerto Rico Trench and eastern Hispaniola (Dominican Republic). Location of the transect is shown on the map in **Fig. 1**. Calculated Bouguer gravity anomalies (thin solid line) are tied to the observed gravity anomalies (thick dashed line) at station 2B (Bunce & Fahlquist 1962) with the residuals shown as the red line. Crustal surfaces were constrained by seismic refraction stations shown by “x” (Ewing *et al.* 1960; Bunce & Fahlquist 1962; Bunce *et al.* 1969). This transect crosses Transect 3 (also shown by “x’). Black dots represent earthquake epicentres with the sizes of the dots indicating the relative magnitudes of the earthquakes. The short vertical lines through the epicentres indicate the available depth errors for the earthquakes. Coloured layers in the crust and mantle correspond to different densities used for the gravity modelling. MT, Muertos Trough; PRT, Puerto Rico Trench.

Fig. 12. Major faults and folds in the Dominican Republic and Haiti (Mann *et al.* 1995; Secretary of Industry and Commerce 2005). The areas of high k_{sn} values shown in yellow are spatially associated with the axes of mapped folds and thrust faults. The oblique convergence direction between North American-Caribbean plates is shown by the large black arrow. The thick yellow line separates the topographically-low eastern Hispaniola area– that overlies subducted slabs of the North American and Caribbean plates – from the topographically-elevated western Hispaniola area – that is undergoing oblique collision and is characterized by large-scale folding and thrusting.

Fig. 13. GPS vectors from Calais et al. (2016) showing plate convergence, crustal shortening, and long-wavelength crustal folding across central and western Hispaniola. The Caribbean plate is held fixed, and vectors show the southwestward displacement of Hispaniola relative to the Caribbean plate. The oblique convergence direction between North American-Caribbean plates known from GPS geodesy is shown by the large black arrow. The thick yellow line separates the topographically-low eastern Hispaniola area from the topographically-elevated western Hispaniola area.

Fig. 14. Earthquake epicentres in the magnitude range of 3.5-7.7 that are colour coded by depth from the USGS ANSS Comprehensive Earthquake Catalogue (U.S. Geological Survey 2019). Earthquake moment tensors are compiled from the global CMT catalogue (Dziewonski *et al.* 1981; Ekström *et al.* 2012). Earthquake magnitudes in the CMT catalogue are scaled according to the relative sizes of the earthquake mechanisms. Earthquake moment tensors south of eastern Hispaniola are labelled and discussed in the text. The oblique convergence direction between North American-Caribbean plates is shown by the large black arrow. The thick yellow line separates the topographically-low, eastern Hispaniola area from the topographically-elevated western Hispaniola area. HM, Hispaniola microplate; NHM, North Hispaniola microplate; PRVIM, Puerto Rico and Virgin Islands microplate.

Fig. 15. The sedimentary thickness of onshore basins in Hispaniola and offshore basins surrounding Hispaniola and Puerto Rico (Tillman and Mann, this volume). The thickness data are gridded from the surface to the interpreted top of crystalline basement and are compiled from 2D seismic reflection lines and regional geologic cross sections (both are shown in magenta). The oblique convergence direction between North American-Caribbean plates is shown by the large black arrow. The thick yellow line separates the topographically-low eastern Hispaniola area from the topographically-elevated western Hispaniola area. EB, Enriquillo Basin; SJB, San Juan Basin; CB, Cibao Basin; HM, Hispaniola microplate; NHM, North Hispaniola microplate; PRVIM, Puerto Rico and Virgin Islands microplate.

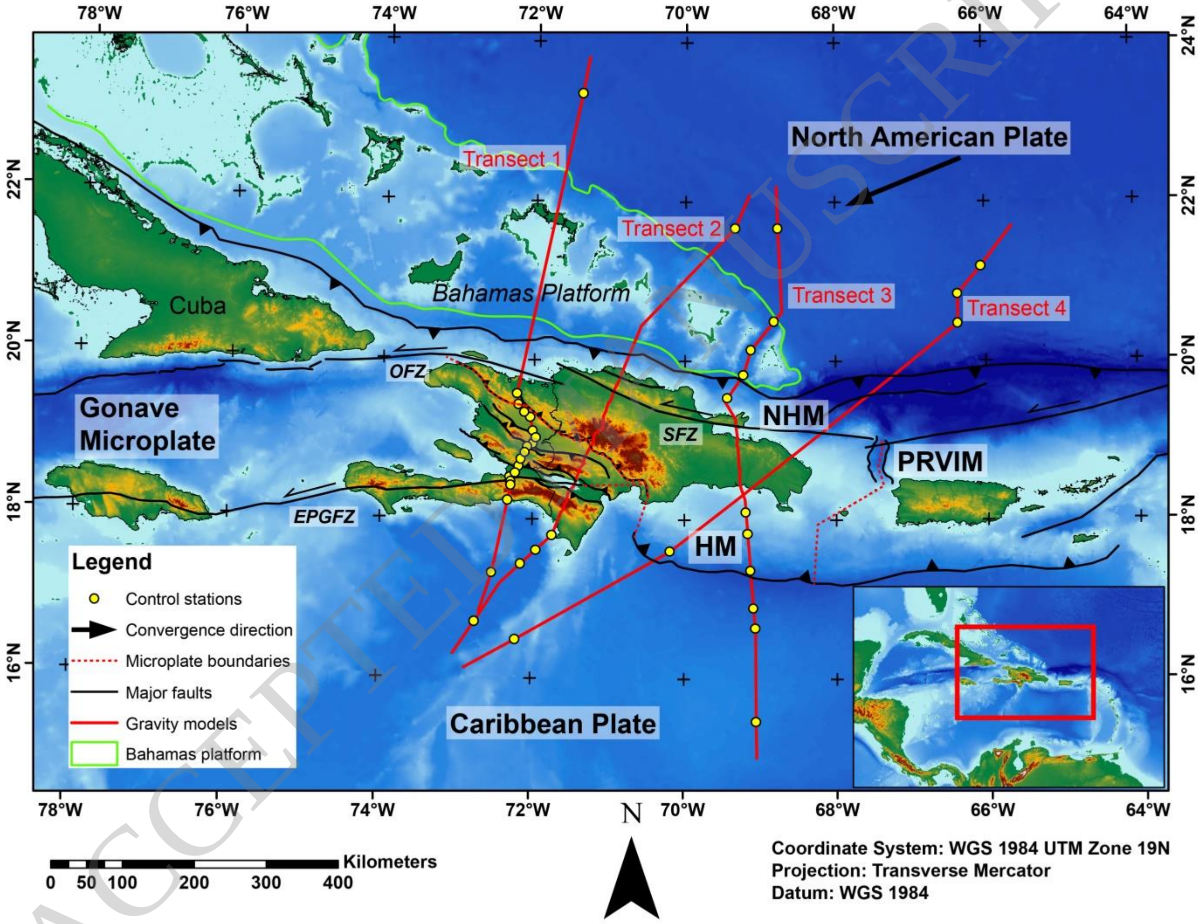

North American Plate
Transect 1
Transect 2
Transect 3
Transect 4
Bahamas Platform
Cuba
OFZ
Gonave Microplate
NHM
SFZ
PRVIM
EPGFZ
HM
Caribbean Plate
Legend
Control stations
Convergence direction
Microplate boundaries
Major faults
Gravity models
Bahamas platform
78°W
76°W
74°W
72°W
70°W
68°W
66°W
64°W
24°N
22°N
20°N
18°N
16°N
N
Kilometers
0 50 100 200 300 400
Coordinate System: WGS 1984 UTM Zone 19N
Projection: Transverse Mercator
Datum: WGS 1984

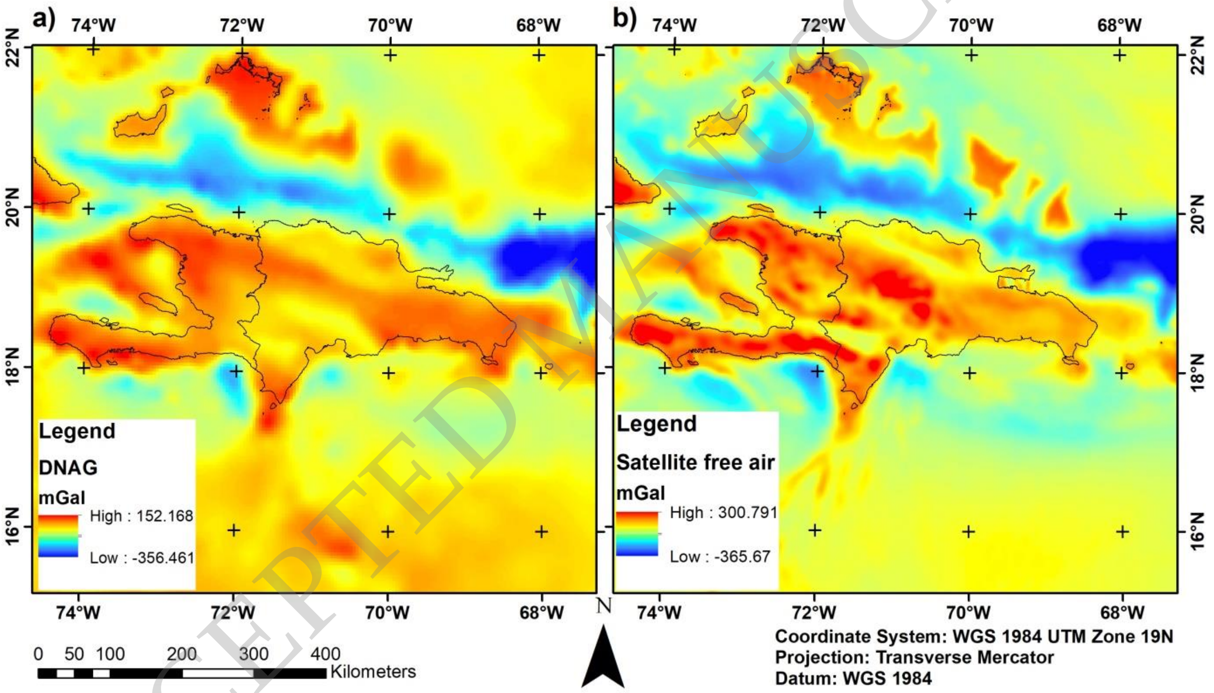
a)
74°W
72°W
70°W
68°W
22°N
20°N
18°N
16°N
Legend
DNAG
mGal
High : 152.168
Low : -356.461
0 50 100 200 300 400
Kilometers
N
b)
Legend
Satellite free air
mGal
High : 300.791
Low : -365.67
Coordinate System: WGS 1984 UTM Zone 19N
Projection: Transverse Mercator
Datum: WGS 1984

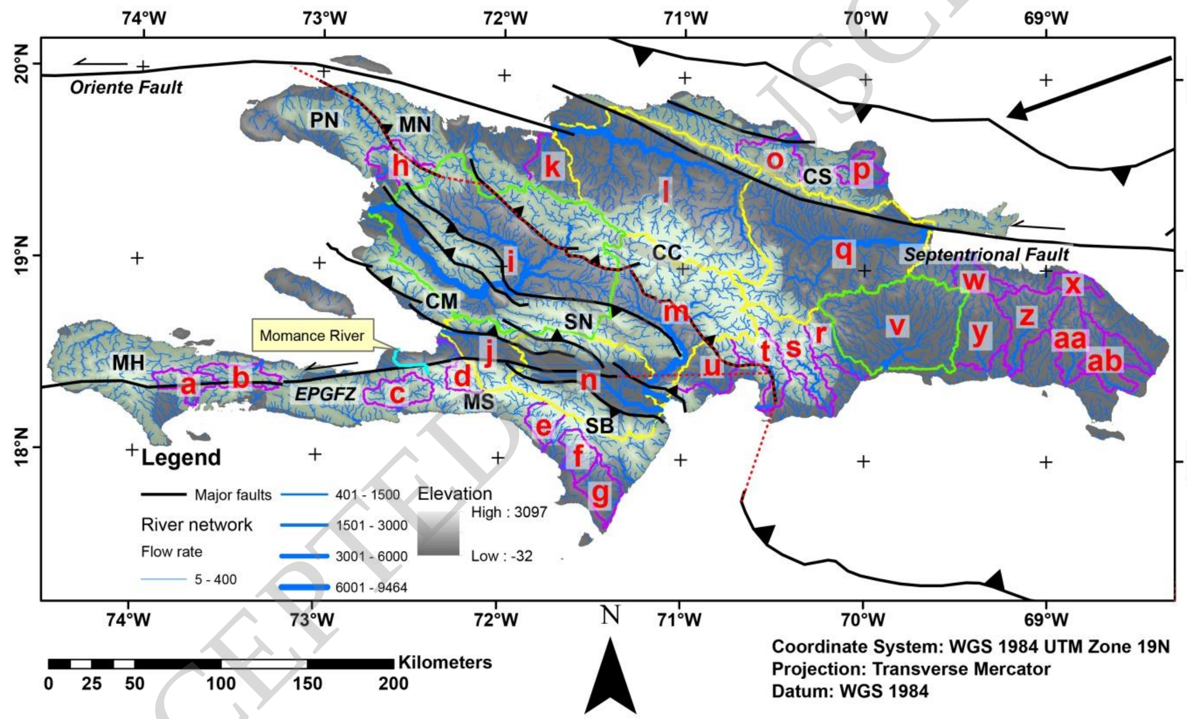
74°W
73°W
72°W
71°W
70°W
69°W
20°N
19°N
18°N
Oriente Fault
Septentrional Fault
EPGFZ
Momance River
PN
MN
CC
CM
SN
MS
SB
MH
CS
a
b
c
d
e
f
g
h
i
j
k
l
m
n
o
p
q
r
s
t
u
v
w
x
y
z
aa
ab
Legend
Major faults
River network
Flow rate
5 - 400
401 - 1500
1501 - 3000
3001 - 6000
6001 - 9464
Elevation
High : 3097
Low : -32
N
Kilometers
0
25
50
100
150
200
Coordinate System: WGS 1984 UTM Zone 19N
Projection: Transverse Mercator
Datum: WGS 1984

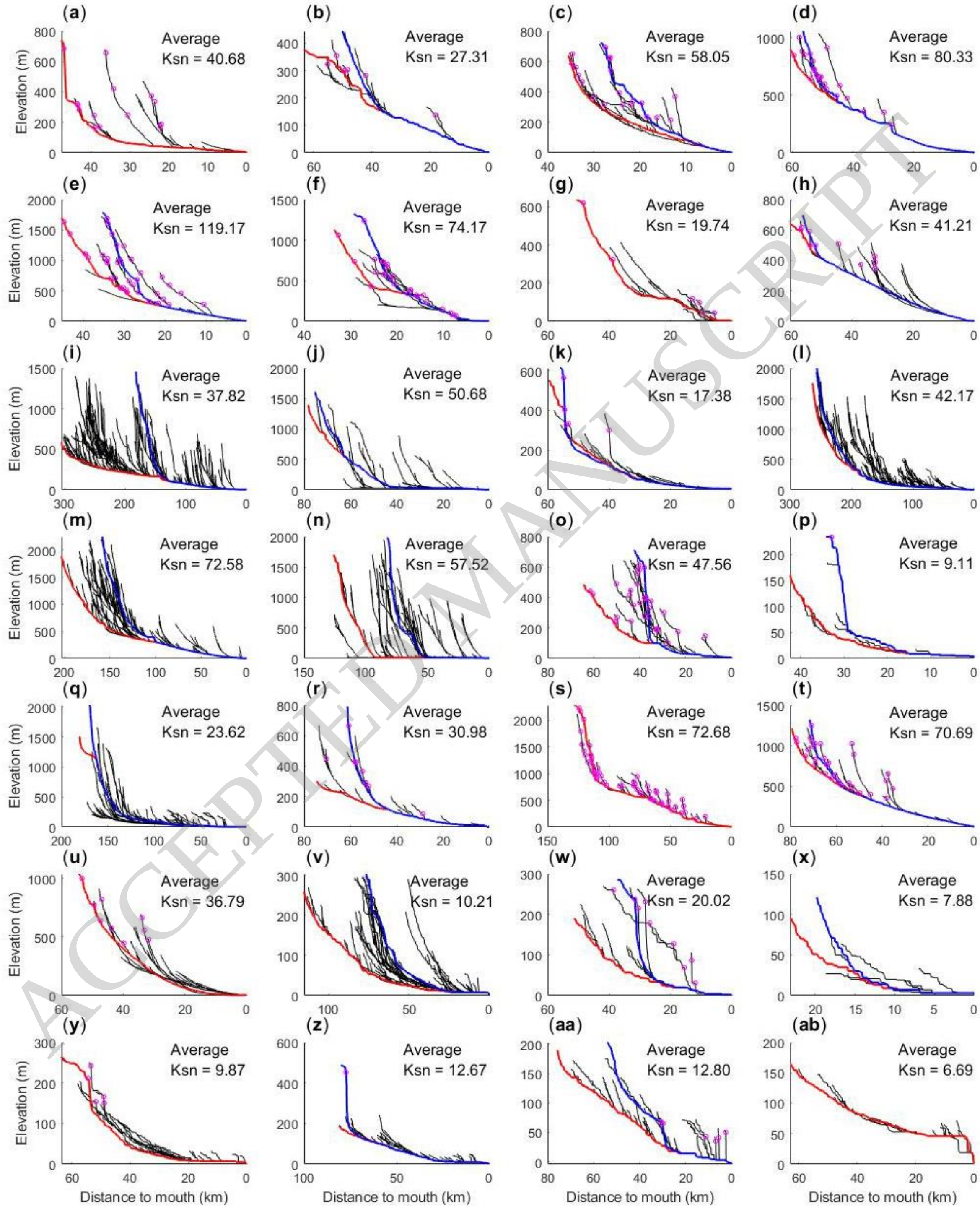
(a)
Average
Ksn = 40.68
(b)
Average
Ksn = 27.31
(c)
Average
Ksn = 58.05
(d)
Average
Ksn = 80.33
(e)
Average
Ksn = 119.17
(f)
Average
Ksn = 74.17
(g)
Average
Ksn = 19.74
(h)
Average
Ksn = 41.21
(i)
Average
Ksn = 37.82
(j)
Average
Ksn = 50.68
(k)
Average
Ksn = 17.38
(l)
Average
Ksn = 42.17
(m)
Average
Ksn = 72.58
(n)
Average
Ksn = 57.52
(o)
Average
Ksn = 47.56
(p)
Average
Ksn = 9.11
(q)
Average
Ksn = 23.62
(r)
Average
Ksn = 30.98
(s)
Average
Ksn = 72.68
(t)
Average
Ksn = 70.69
(u)
Average
Ksn = 36.79
(v)
Average
Ksn = 10.21
(w)
Average
Ksn = 20.02
(x)
Average
Ksn = 7.88
(y)
Average
Ksn = 9.87
(z)
Average
Ksn = 12.67
(aa)
Average
Ksn = 12.80
(ab)
Average
Ksn = 6.69
Elevation (m)
Distance to mouth (km)

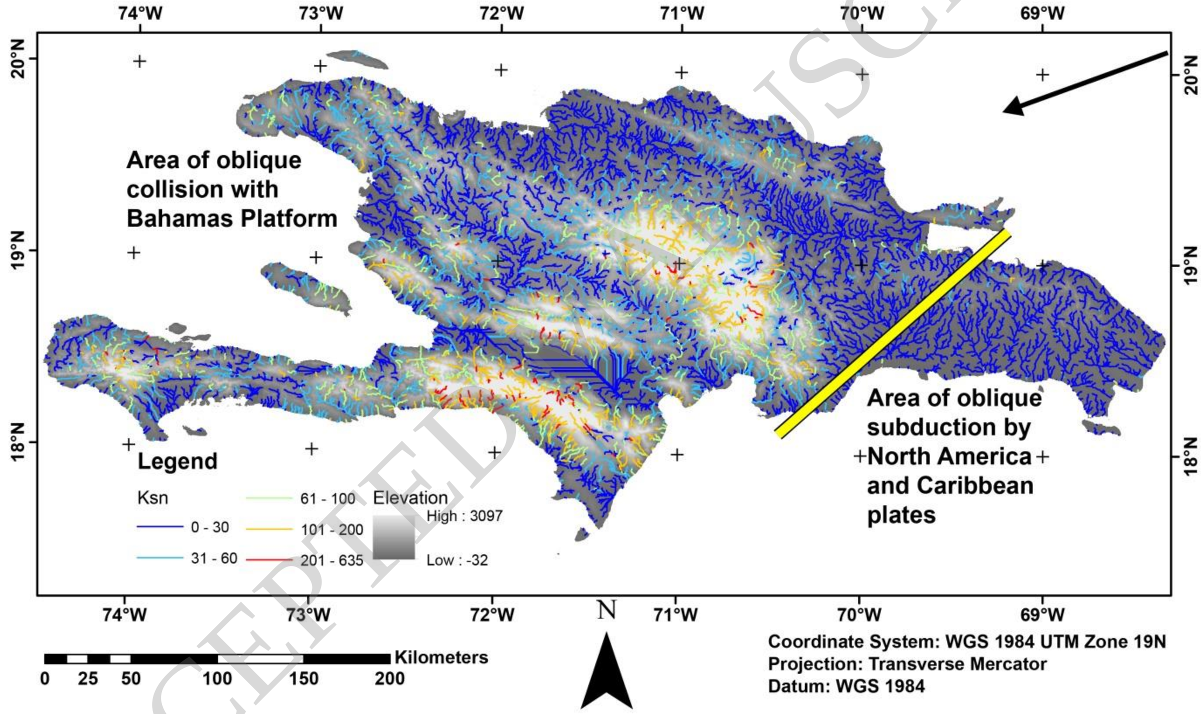
74°W
73°W
72°W
71°W
70°W
69°W
20°N
19°N
18°N
Area of oblique collision with Bahamas Platform
Area of oblique subduction by North America and Caribbean plates
Legend
Ksn
0 - 30
31 - 60
61 - 100
101 - 200
201 - 635
Elevation
High : 3097
Low : -32
Kilometers
0 25 50 100 150 200
N
Coordinate System: WGS 1984 UTM Zone 19N
Projection: Transverse Mercator
Datum: WGS 1984

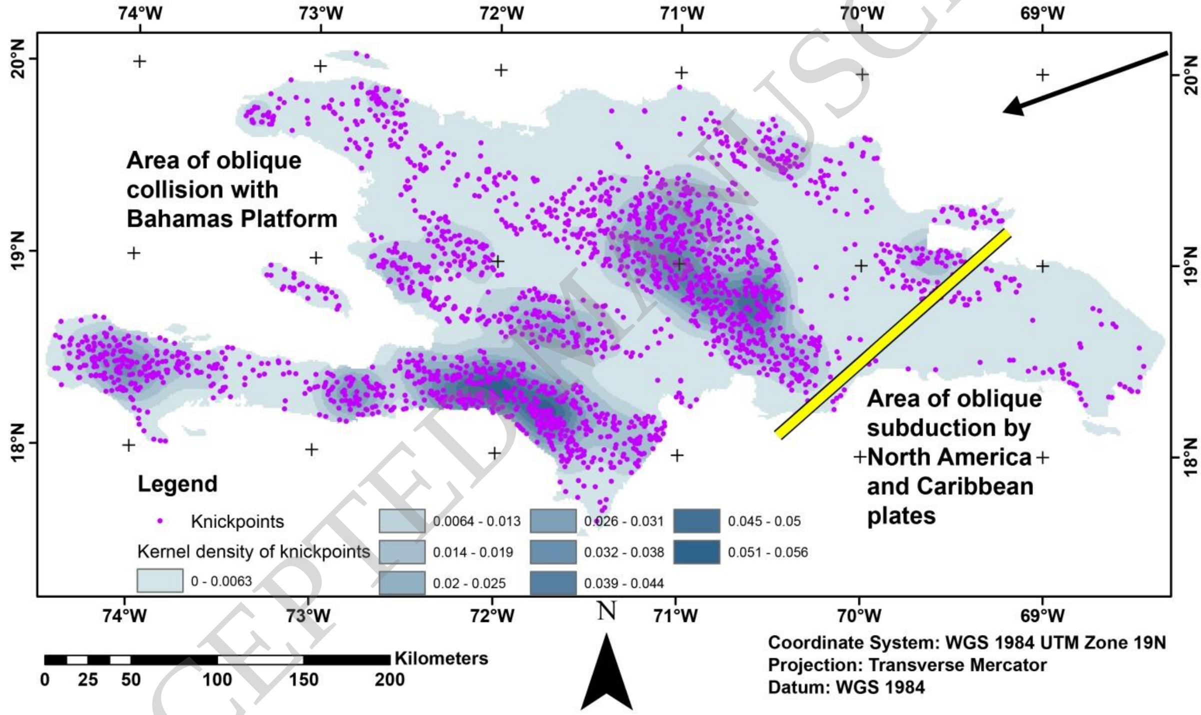
74°W
73°W
72°W
71°W
70°W
69°W
20°N
19°N
18°N
Area of oblique collision with Bahamas Platform
Area of oblique subduction by North America and Caribbean plates
Legend
Knickpoints
Kernel density of knickpoints
0 - 0.0063
0.0064 - 0.013
0.014 - 0.019
0.02 - 0.025
0.026 - 0.031
0.032 - 0.038
0.039 - 0.044
0.045 - 0.05
0.051 - 0.056
Kilometers
0 25 50 100 150 200
N
Coordinate System: WGS 1984 UTM Zone 19N
Projection: Transverse Mercator
Datum: WGS 1984

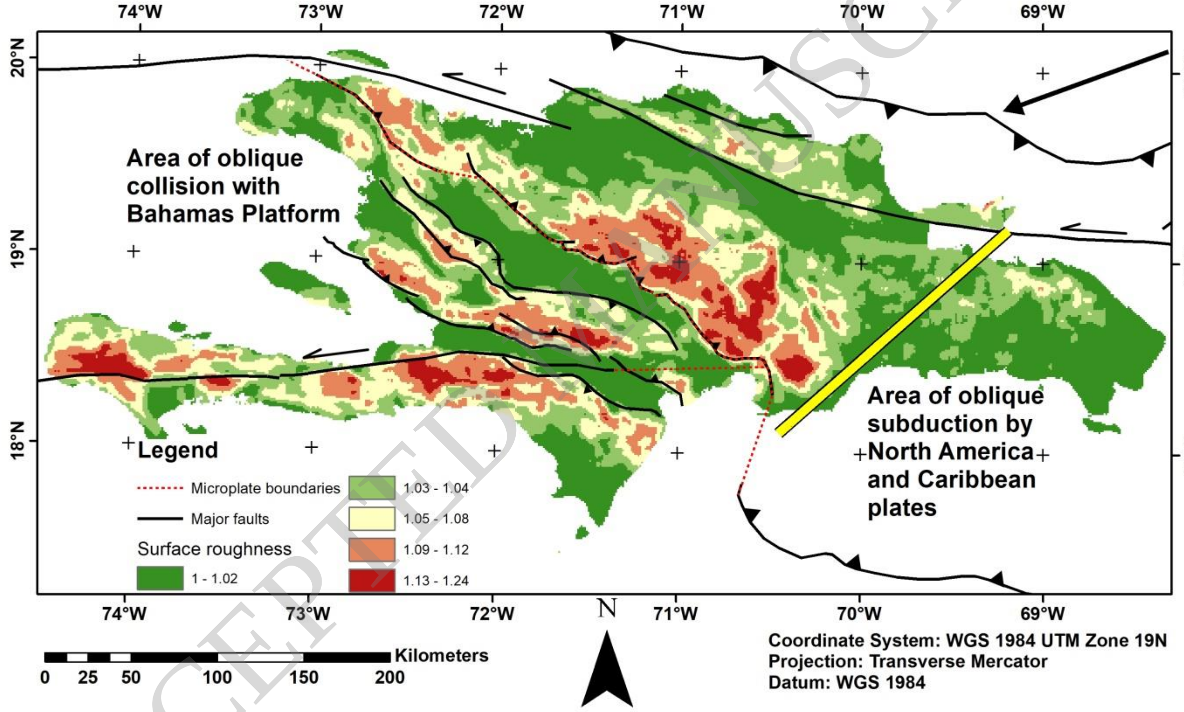

74°W
73°W
72°W
71°W
70°W
69°W
20°N
19°N
18°N
Area of oblique collision with Bahamas Platform
Area of oblique subduction by North America and Caribbean plates
Legend
Microplate boundaries
Major faults
Surface roughness
1 - 1.02
1.03 - 1.04
1.05 - 1.08
1.09 - 1.12
1.13 - 1.24
Kilometers
0 25 50 100 150 200
N
Coordinate System: WGS 1984 UTM Zone 19N
Projection: Transverse Mercator
Datum: WGS 1984

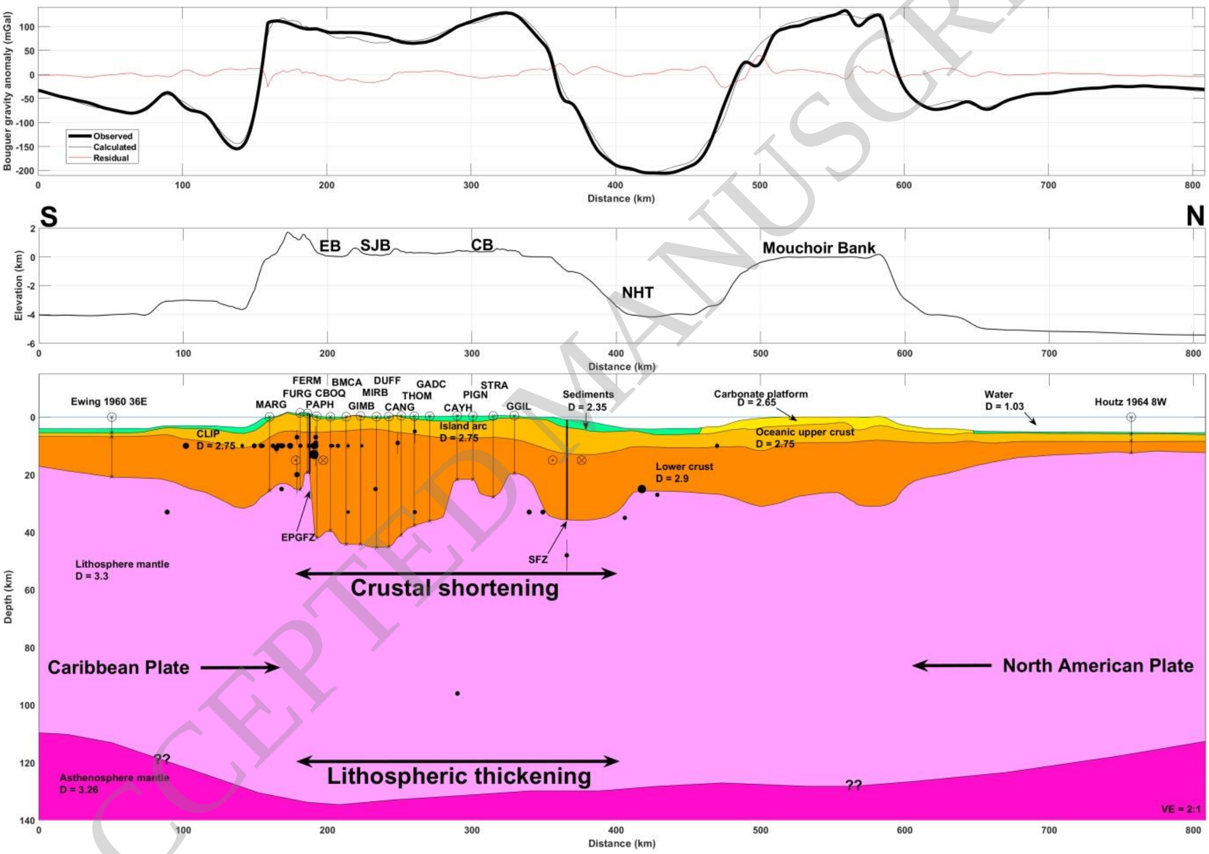
Bouguer gravity anomaly (mGal)
Observed
Calculated
Residual
Distance (km)
S
N
EB
SJB
CB
Mouchoir Bank
NHT
Elevation (km)
Ewing 1960 36E
MARG
FERM
FURG CBOQ
PAPH
BMCA
MIRB
GIMB
DUFF
CANG
GADC
THOM
CAYH
STRA
PIGN
GGIL
Sediments
D = 2.35
Carbonate platform
D = 2.65
Water
D = 1.03
Houtz 1964 8W
CLIP
D = 2.75
Island arc
D = 2.75
Oceanic upper crust
D = 2.75
Lower crust
D = 2.9
EPGFZ
SFZ
Lithosphere mantle
D = 3.3
Crustal shortening
Caribbean Plate
North American Plate
Lithospheric thickening
Asthenosphere mantle
D = 3.26
??
VE = 2:1
Depth (km)

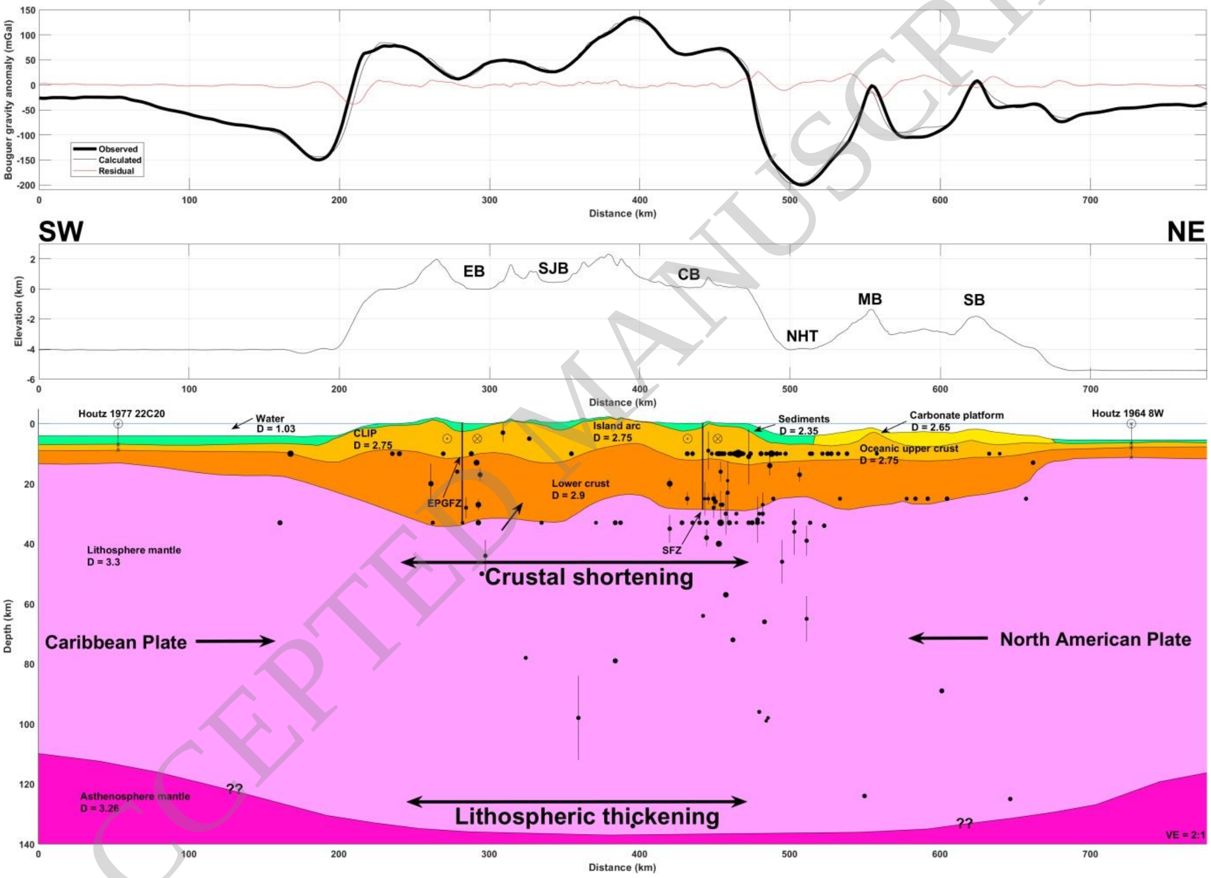
Bouguer gravity anomaly (mGal)
Observed
Calculated
Residual
Distance (km)
SW
NE
Elevation (km)
EB
SJB
CB
NHT
MB
SB
Houtz 1977 22C20
Water
D = 1.03
CLIP
D = 2.75
Island arc
D = 2.75
Sediments
D = 2.35
Carbonate platform
D = 2.65
Houtz 1964 8W
Oceanic upper crust
D = 2.75
Lower crust
D = 2.9
EPGFZ
SFZ
Lithosphere mantle
D = 3.3
Crustal shortening
Depth (km)
Caribbean Plate
North American Plate
Asthenosphere mantle
D = 3.26
??
Lithospheric thickening
VE = 2:1

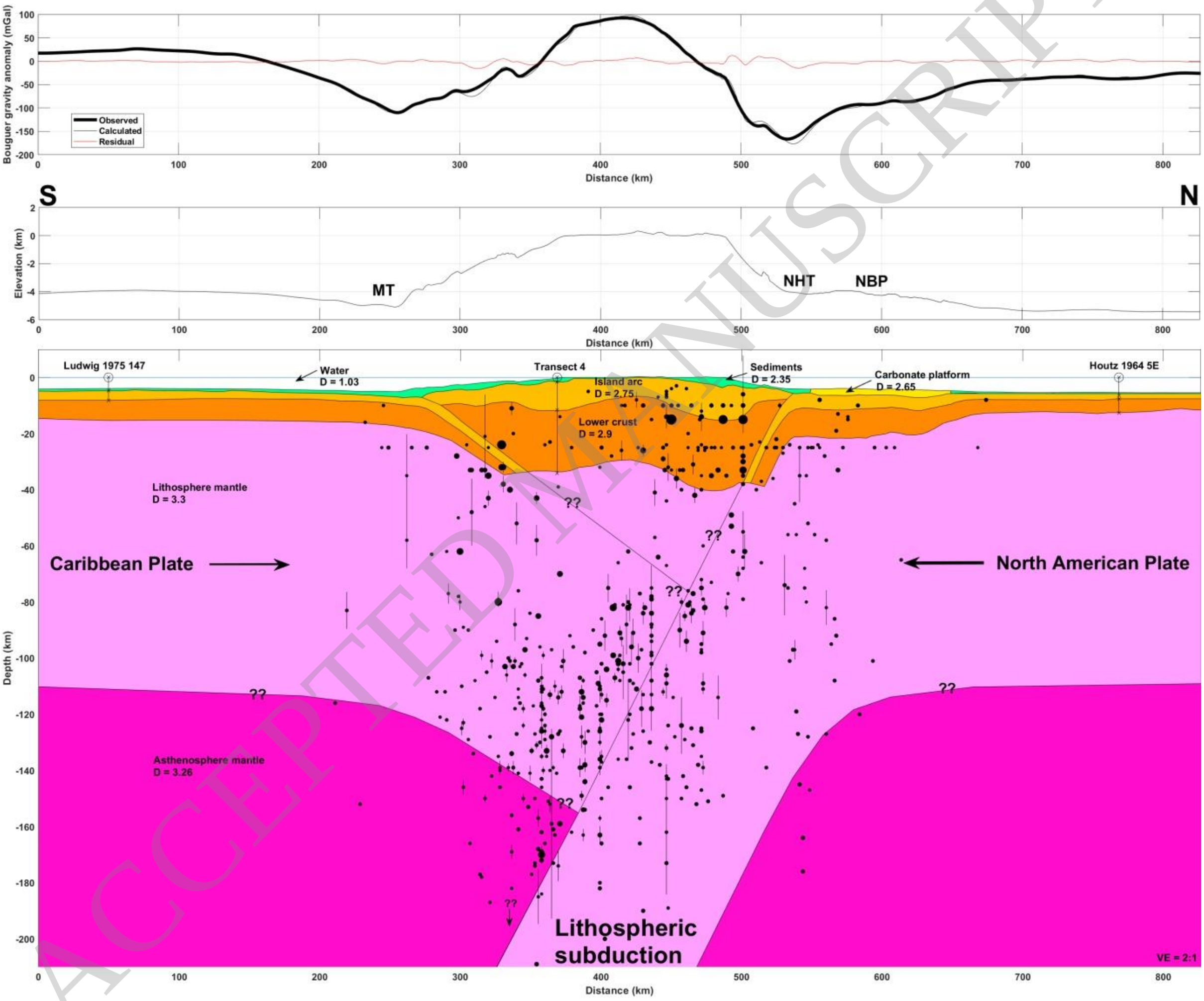

Bouguer gravity anomaly (mGal)
Observed
Calculated
Residual
Distance (km)
S
N
Elevation (km)
MT
NHT
NBP
Distance (km)
Ludwig 1975 147
Water
D = 1.03
Transect 4
Island arc
D = 2.75
Sediments
D = 2.35
Carbonate platform
D = 2.65
Houtz 1964 5E
Lower crust
D = 2.9
Lithosphere mantle
D = 3.3
Caribbean Plate
North American Plate
Asthenosphere mantle
D = 3.26
Lithospheric
subduction
Depth (km)
VE = 2:1
Distance (km)

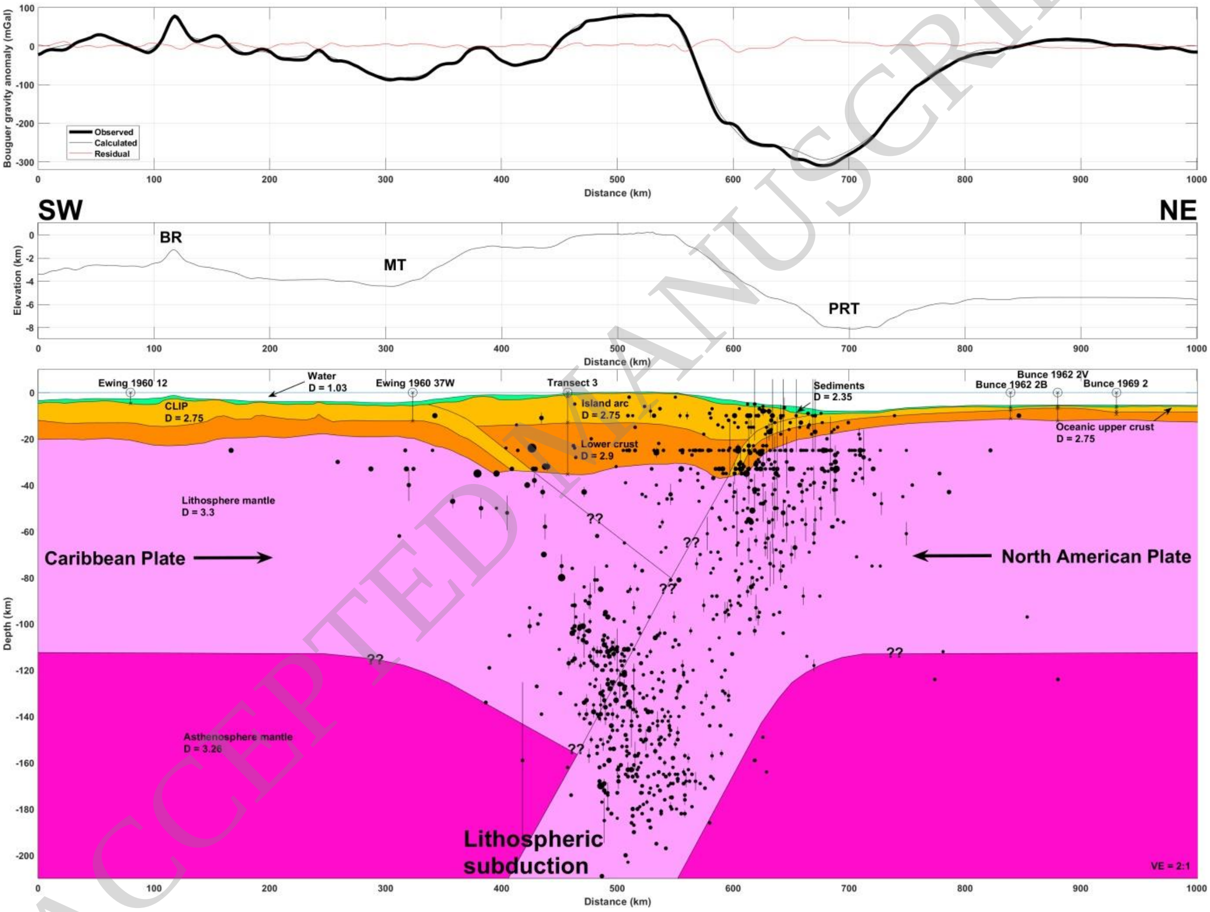

Bouguer gravity anomaly (mGal)
Observed
Calculated
Residual
Distance (km)
SW
NE
BR
MT
PRT
Elevation (km)
Distance (km)
Ewing 1960 12
Water
D = 1.03
Ewing 1960 37W
Transect 3
Sediments
D = 2.35
Bunce 1962 2V
Bunce 1962 2B
Bunce 1969 2
CLIP
D = 2.75
Island arc
D = 2.75
Lower crust
D = 2.9
Oceanic upper crust
D = 2.75
Lithosphere mantle
D = 3.3
Caribbean Plate
North American Plate
Asthenosphere mantle
D = 3.26
Lithospheric
subduction
Depth (km)
VE = 2:1
Distance (km)

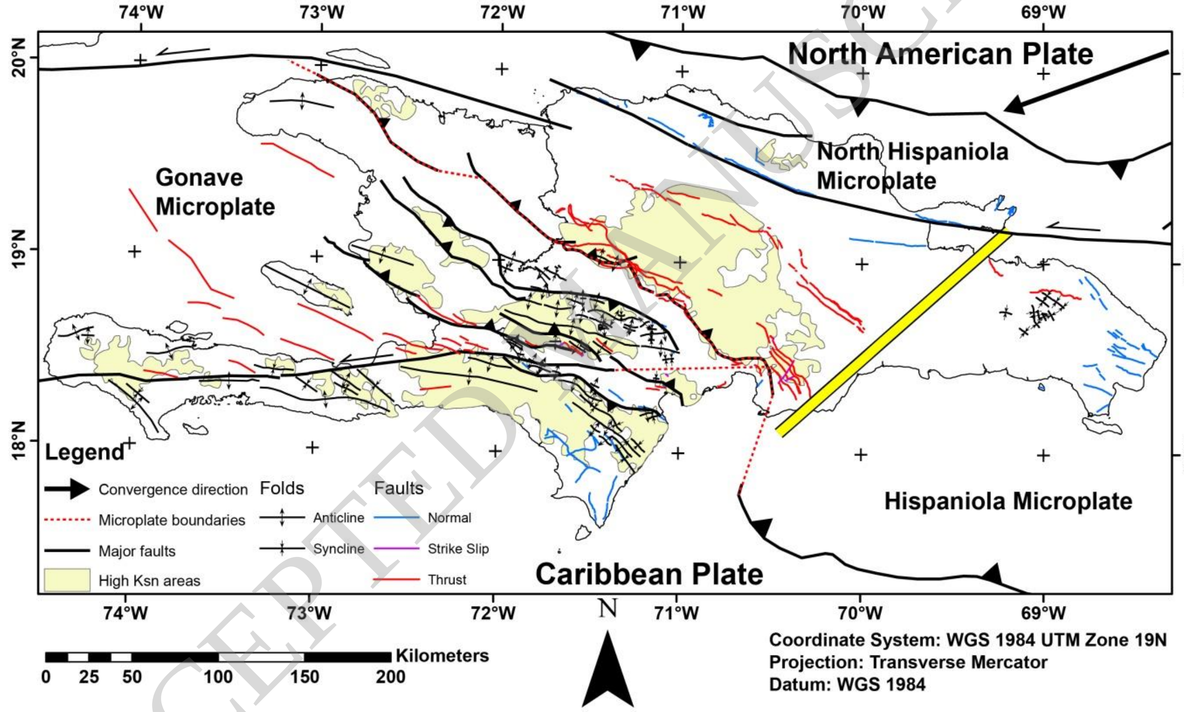
74°W
73°W
72°W
71°W
70°W
69°W
20°N
19°N
18°N
North American Plate
North Hispaniola
Microplate
Gonave
Microplate
Hispaniola Microplate
Caribbean Plate
Legend
Convergence direction
Microplate boundaries
Major faults
High Ksn areas
Folds
Anticline
Syncline
Faults
Normal
Strike Slip
Thrust
Kilometers
0 25 50 100 150 200
N
Coordinate System: WGS 1984 UTM Zone 19N
Projection: Transverse Mercator
Datum: WGS 1984

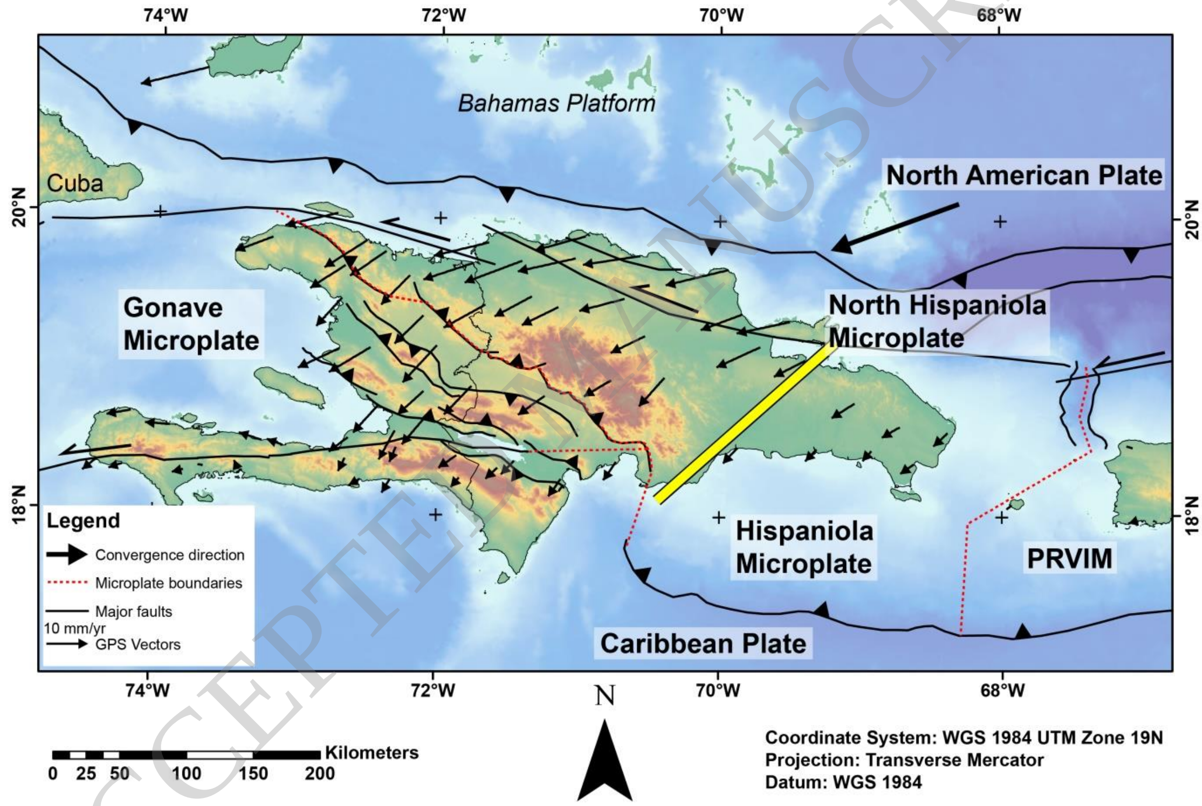
74°W
72°W
70°W
68°W
Bahamas Platform
Cuba
North American Plate
20°N
Gonave
Microplate
North Hispaniola
Microplate
Hispaniola
Microplate
PRVIM
Caribbean Plate
18°N
Legend
Convergence direction
Microplate boundaries
Major faults
10 mm/yr
GPS Vectors
0 25 50 100 150 200
Kilometers
N
Coordinate System: WGS 1984 UTM Zone 19N
Projection: Transverse Mercator
Datum: WGS 1984

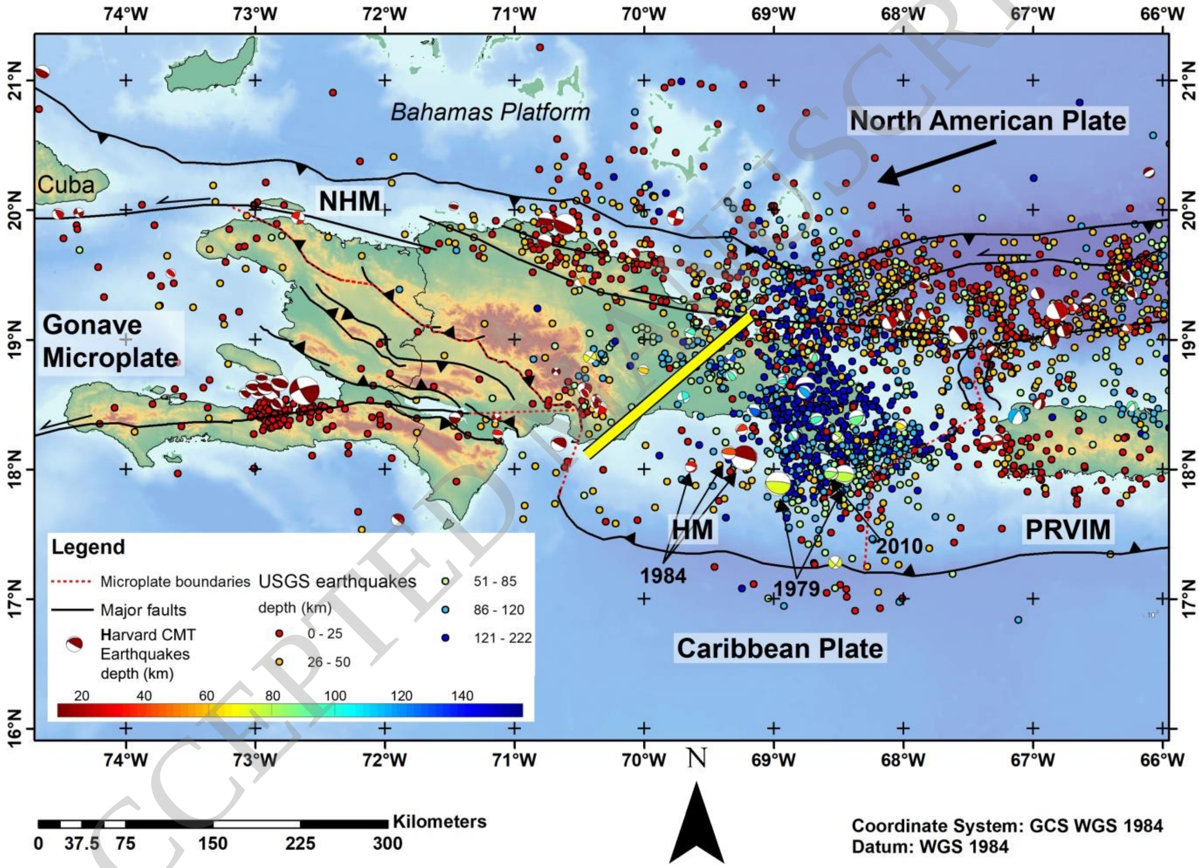

74°W
73°W
72°W
71°W
70°W
69°W
68°W
67°W
66°W
21°N
20°N
19°N
18°N
17°N
16°N
Bahamas Platform
North American Plate
Cuba
NHM
Gonave
Microplate
HM
1984
1979
2010
PRVIM
Caribbean Plate
Legend
Microplate boundaries
Major faults
Harvard CMT
Earthquakes
depth (km)
USGS earthquakes
depth (km)
0 - 25
26 - 50
51 - 85
86 - 120
121 - 222
20
40
60
80
100
120
140
Kilometers
0
37.5
75
150
225
300
N
Coordinate System: GCS WGS 1984
Datum: WGS 1984

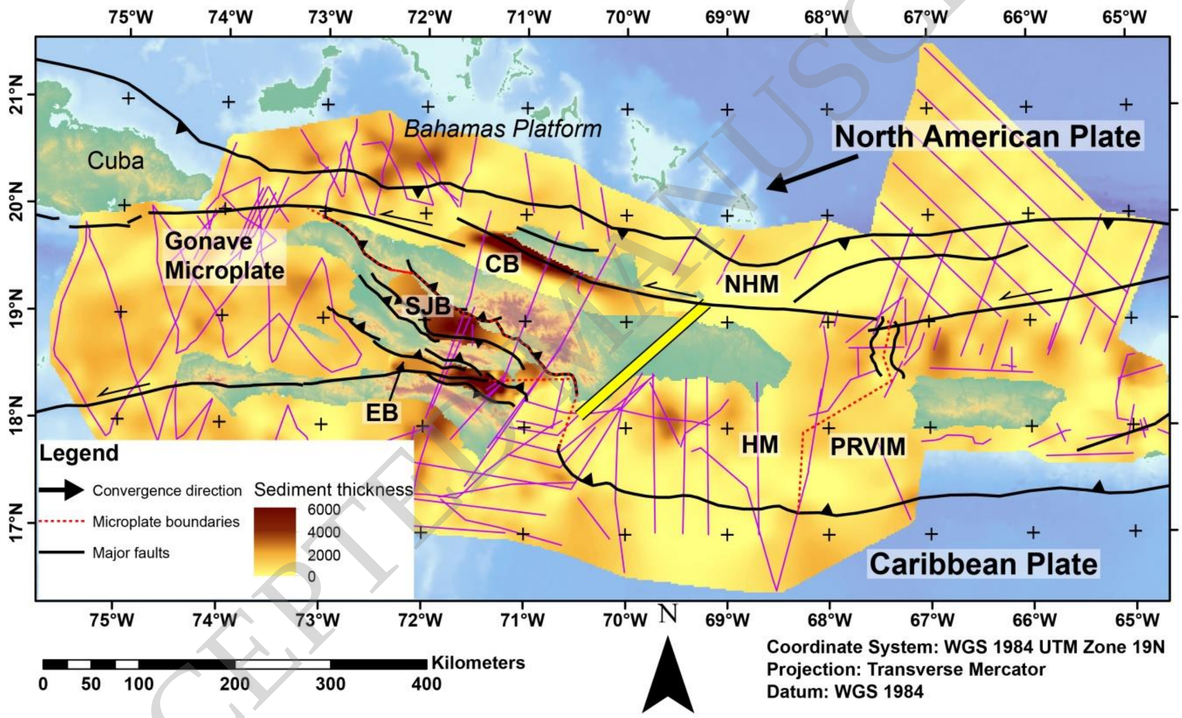
75°W
74°W
73°W
72°W
71°W
70°W
69°W
68°W
67°W
66°W
65°W
21°N
20°N
19°N
18°N
17°N
Bahamas Platform
Cuba
North American Plate
Gonave
Microplate
CB
NHM
SJB
EB
HM
PRVIM
Caribbean Plate
Legend
Convergence direction
Microplate boundaries
Major faults
Sediment thickness
6000
4000
2000
0
Kilometers
0 50 100 200 300 400
N
Coordinate System: WGS 1984 UTM Zone 19N
Projection: Transverse Mercator
Datum: WGS 1984